REVIEW ARTICLE (INVITED ONLY)

Recent Advances on the Luminescent Solar Concentrator Employing Quantum Dots

Jiwon Song[1] · Chanwoo Kim[1] · Subin Lee[1] · Hangil Lee[1] · Jeongin Seo[1] · Hyung-Jun Song[1]

Abstract

The advent of quantum dots (QDs) enables us to reshape the incident light spectrum through absorption and re-emission. By exploiting the distinctive optical properties of QDs, a diverse array of optoelectronic devices that integrate QDs, including light-emitting diodes, solar cells, optical filters, and other applications, have gained widespread acceptance. Among promising applications for energy generation, luminescent solar concentrators (LSCs) exhibit remarkable potential, where QDs absorb incident solar light and re-emit it through QDs waveguides to edge-mounted solar cells. The substantial Stokes shift of QDs effectively mitigates addressed issues related to reabsorption, and the utilization of solution-processed QDs facilitates the development of low-cost LSCs. Consequently, considerable research efforts have been directed toward the development of QD-based LSCs, aiming to harness solar light more efficiently at reduced costs. This review systematically examines the potential of QD-based LSCs as a future energy solution and optical devices. It delves into the operating principles, theoretically attainable energy, materials, and optical structure developments, as well as potential applications of LSCs. Additionally, the review discusses challenges associated with QD–LSCs and outlines future research directions. We believe that this comprehensive review provides insights into the current status and prospects of LSCs employing QDs, serving as a valuable resource for researchers and professionals in the field.

Keywords Quantum dot · Luminescent solar concentrator · Down-shifting · Building integrated photovoltaics · Agrivolatics

Introduction

Colloidal quantum dots (QDs) are soluble semiconducting nanocrystals with sizes on the nanometer scale. The control over materials, annealing time, and concentration precursor enables the customization of QD size and shape [1–4]. The optical and electrical properties of QDs are easily tuned by controlling their size and shape, owing to their strong quantum confinement effect. Additionally, ligand exchange of QDs can modify the energy level to a desirable value [5]. Consequently, the attainable advantages of QDs lie in their ability to tune energy levels through synthesis processes and materials, making them a strong candidate for optoelectronic devices, which are extremely challenging to obtain through bulk materials. The unique optical

and electrical properties of QDs broaden their applications, spanning from light-emitting diodes (LEDs) [6–9], solar energy-harvesting [10], field-effect transistors [11], medical imaging [12], optical filters [13], and lasers [14]. The QD-enhanced LEDs have successfully entered the market and are competing with other technologies in the high-end display sector [15–17]. As QDs have entered the market, there has been a significant reduction in fabrication costs and upscaling of the synthesis procedure. While other possible applications have been developed at the lab scale, they face challenges in commercialization [18]. The development of the roll-to-roll and coating processes has decreased the energy consumption and costs associated with QD film casting on various substrates [19]. Furthermore, the lowered process temperatures have expanded the range of possible substrates from rigid glass substrates to flexible polymer films [20]. Furthermore, the introduction of inkjet printing technology to QDs allows patterns of different kinds of layers on desirable areas [21, 22], enabling the manufacture of complex electronic devices through low-temperature processes using soluble QDs. With advances in the synthesis

✉ Hyung-Jun Song
  hj.song@seoultech.ac.kr

1 Department of Safety Engineering, Seoul National University of Science and Technology, Seoul 01811, Republic of Korea

and manufacturing of QDs, the realization of low-cost but highly efficient optoelectronic devices incorporating QDs is becoming increasingly feasible.

Among the many advantages of QDs, their large Stokes shift is a highly desirable feature for leveraging down-shifting layers in optoelectronic devices [23–26]. The quantum confinement effect, arising from confining charge carriers within the small dimensions of QDs, leads to discrete energy levels. The energy levels associated with absorption and emission are influenced differently by the quantum confinement effect, resulting in a larger Stokes shift of QDs. Moreover, QDs with core/shell structures, composed of two different materials, minimize spectral overlap between absorption and emission [27, 28]. The outer shell with a wide band gap absorbs high-energy photons, while the core emits low-energy photons via internal energy transfer. Exploiting this unique optical property of QDs allows for reshaping the incident light spectrum, enabling applications such a. full-colored LEDs [4], colorful solar cells [23, 29], and biomarkers [12, 30] using QD films. The expansion of QD applications has reached a point to demonstrate an energy-generating window, which is called a luminescent solar concentrator (LSC) [31–33].

The LSC comprises a waveguide plate integrated with luminophores, which absorb incident solar light and re-emit the light with low-energy photons. Given the excellent down-shifting properties of QDs, they emerge as a strong candidate for luminophore in the LSC. Usually, solution-processed QDs are coated or integrated into a relatively simple substrate made of glass or plastic plates. This substrate aids in guiding the re-emitted photons toward the edge of glass or polymer slabs. Then, edge-mounted photovoltaic cells (PVs) convert waveguided light into electricity [34]. LSCs can be directly connected to existing PVs without further modifications (Fig. 1(a)) [35]. Consequently, by concentrating weak light and reshaping the solar spectrum in the LSC, PVs equipped with LSCs can generate more energy compared to those without them. Moreover, the performance of LSC remains mostly independent of incident angles, enabling effective operation even under non-normal incident illumination. Introducing LSC technology to PV systems reduces the necessity for expensive tracking systems, thus promoting the realization of a cost-effective energy-harvesting system. According to recent studies, the commercial viability of QD–LSCs hinges on their cost being half that of PVs over a lifetime. This affordability renders them suitable for energy-harvesting in densely populated urban areas as they allow visible light to pass without distortion [36]. Consequently, the QD–LSCs have found application in building integrated photovoltaics (BIPVs), converting building facades and windows into electricity generators (Fig. 1(b) and (c)) [37, 38]. They also facilitate energy-harvesting in agriculture, such as in a greenhouse employing LSC [39], providing diverse opportunities for solar energy utilization.
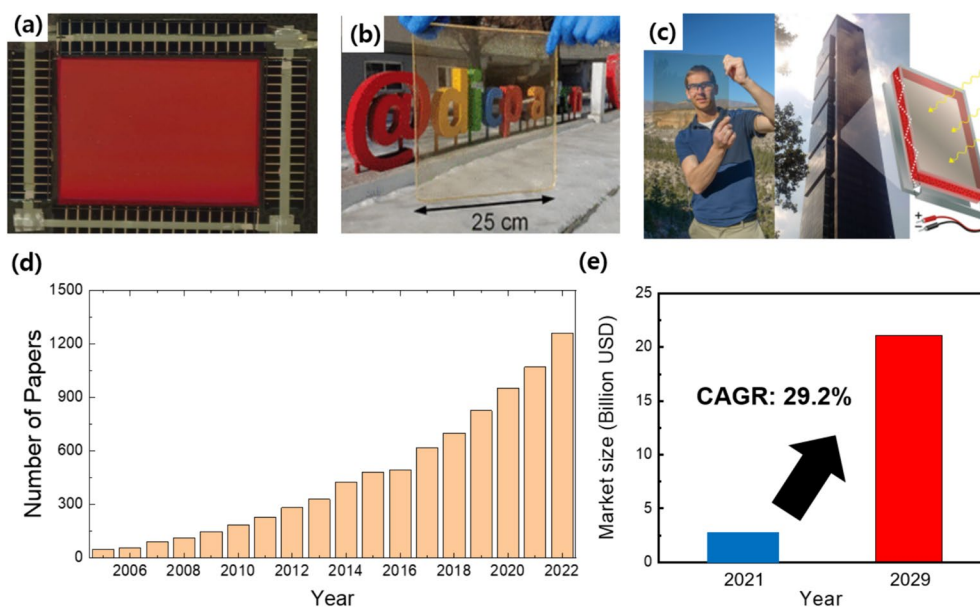
Fig. 1 a Photograph of (a) LSC with PVs (Reprinted with permission [35]. Copyright 2015, Wile-VCH), **b** transparent LSC for window applications (Reprinted with permission [37], Copyright 2022, American Chemical Society), and **c** LSC-based energy-harvesting window for BIPV (Reprinted with permission [38], Copyright 2018, American Chemical Society). **d** The number of published papers related to LSC (Search for papers with title including "Quantum dot Luminescent solar concentrator" through the Google Scholar.) **e** The forecast of global luminescent solar concentrator market estimated by the Data Bridge Market Research in 2022

The energy-harvesting potential of LSCs through transparent substrates has motivated many research groups to study them for more than four decades [40–43]. The sudden surge in fuel prices and the heightened awareness of renewable energy have brought considerable attention to LSC research. LSC became technologically feasible in line with advancements in luminophores and PVs in 2000. Particularly, the emergence of QDs providing redshift emissions has sparked renewed interest in LSC research. There has been a notable increase in research interest, leading to a substantial growth in studies on LSC, as shown in Fig. 1(d). Since 2020, more than 1,000 papers have been consistently published annually, driving significant progress in the performance of LSCs and related materials. It is expected that more papers related with QD-based LSC will be published, which might lead to progress of its performance and stability. Current research endeavors are focused on achieving economically viable QD–LSC by enhancing power conversion efficiency and promoting low-cost, environmentally friendly materials. According to the market trend reports from the Data Bridge Market Research, a compound annual growth rate (CAGR) of LSC-related market will be 29.2% between 2021 and 2029. The report projected that LSC-related markets, such as materials, light-weighted solar cells, and building energy management, will expand rapidly and reach over 29.2 billion USD in 2029, as displayed in Fig. 1(e). The development of luminophores, optical structures, energy management systems, and solar cells will drive the commercialization of LSC.

Given the progress in QD–LSC technology, it is valuable to assess the current state and possible applications of QD–LSC technologies for future research endeavors. This review aims to delve into the recent progress in QD–LSCs. First, the working principle of QD–LSCs is elucidated to understand how it works. Subsequently, we discuss the theoretically achievable energy output through QD–LSCs. Moreover, we review the progress in luminophores and optical structures for efficient QD–LSCs. Finally, we discuss possible applications for LSC, including BIPV, optical communication, and agriculture.

Operating Mechanism of LSCs and Theoretically Attainable Energy

In Fig. 2(a), the operating and loss mechanisms of LSC are depicted. The primary function of LSCs is to absorb incident light and transfer re-emitted photons to edge-mounted PVs. Photons reaching the PV and contributing to electricity generation are denoted as (2c) in Fig. 1(a). In an ideal LSC, luminophores would absorb all incident photons, and the re-emitted light waveguides into the PVs without any optical losses due to internal reflection caused by differences in refractive indices between the air and LSC layer. However, losses inevitably occur due to reflection, re-absorption, imperfect luminophores, and poor out-coupling efficiency. Understanding these mechanisms is crucial for optimizing LSC performance. This chapter analyzes the operating mechanism of LSCs and their theoretical limits resulting from the loss.

A portion of the incident solar radiation ($\sim 4\%$) is reflected at the top surface of the LSC due to the refractive index mismatch between air and the LSC layer (marked as (1c) in Fig. 2(a)) [44]. Some of the incident light passes the LSC without being absorbed by the luminophores (1a). These reflected and unabsorbed photons cannot contribute to the energy generation of LSC. The luminescent layer absorbs other incident light (1b in Fig. 2a), characterized by a bandgap larger than that of luminophores. Upon absorption, the absorbed light is re-emitted to a longer wavelength, propagating through the waveguide media, and ultimately converted into electricity at integrated PVs (2c). However, due to the photoluminescence quantum yield (η_{PLQY}) of the luminophore not being unity, a portion of the absorbed photons is lost (2a). Typically, the refractive index of the LSC plate ($n_{LSC} = 1.5$–1.8) is higher than that of air ($n_{air} = 1$), ensuring that most re-emitted photons reaching the surface are reflected and proceed toward the PVs. In the case of the glass-air interface, the critical angle, an angle of incidence transmitted without reflection, is 42° ($= \sin^{-1}(n_{air}/n_{LSC}) = \sin^{-1}(1/1.5)$). Therefore, light with an incident angle $> 42°$ remains confined within the flat LSC and continues to travel to the PVs due to total internal reflection. At the flat slab of LSC, the trapping efficiency (η_{trap}) of re-emitted light accounts for $\sim 75\%$ of incident photons, considering the solid angle subtended by the total internal reflection cone [45], while $\sim 25\%$ of incident photons escape from the LSC (2b) without undergoing conversion into electricity. During the path to the PVs, multiple instances of total internal reflection occur, which contributes to trapping the photons within the LSC. However, not all entrapped photons are harnessed at the edge-mounted PVs due to reabsorption losses. The overlap between the absorption and emission spectra of luminophores leads to the re-absorption of re-emitted light, resulting in additional losses in the LSC. As previously mentioned, the unavoidable loss of re-absorbed photons, due to the non-unity η_{PLQY} of luminophores, is a significant factor (3a). Furthermore, the trajectory of re-emitted light changes after the re-absorption and re-emission process, thereby increasing the likelihood of escaping from the LSC (3b). To achieve highly efficient LSCs, it is imperative to enhance the proportion of waveguided photons reaching the PVs while simultaneously mitigating losses arising from unabsorbed, re-absorbed, and escaped photons. Consequently, selecting the optimal area for maximizing efficiency and economic viability is
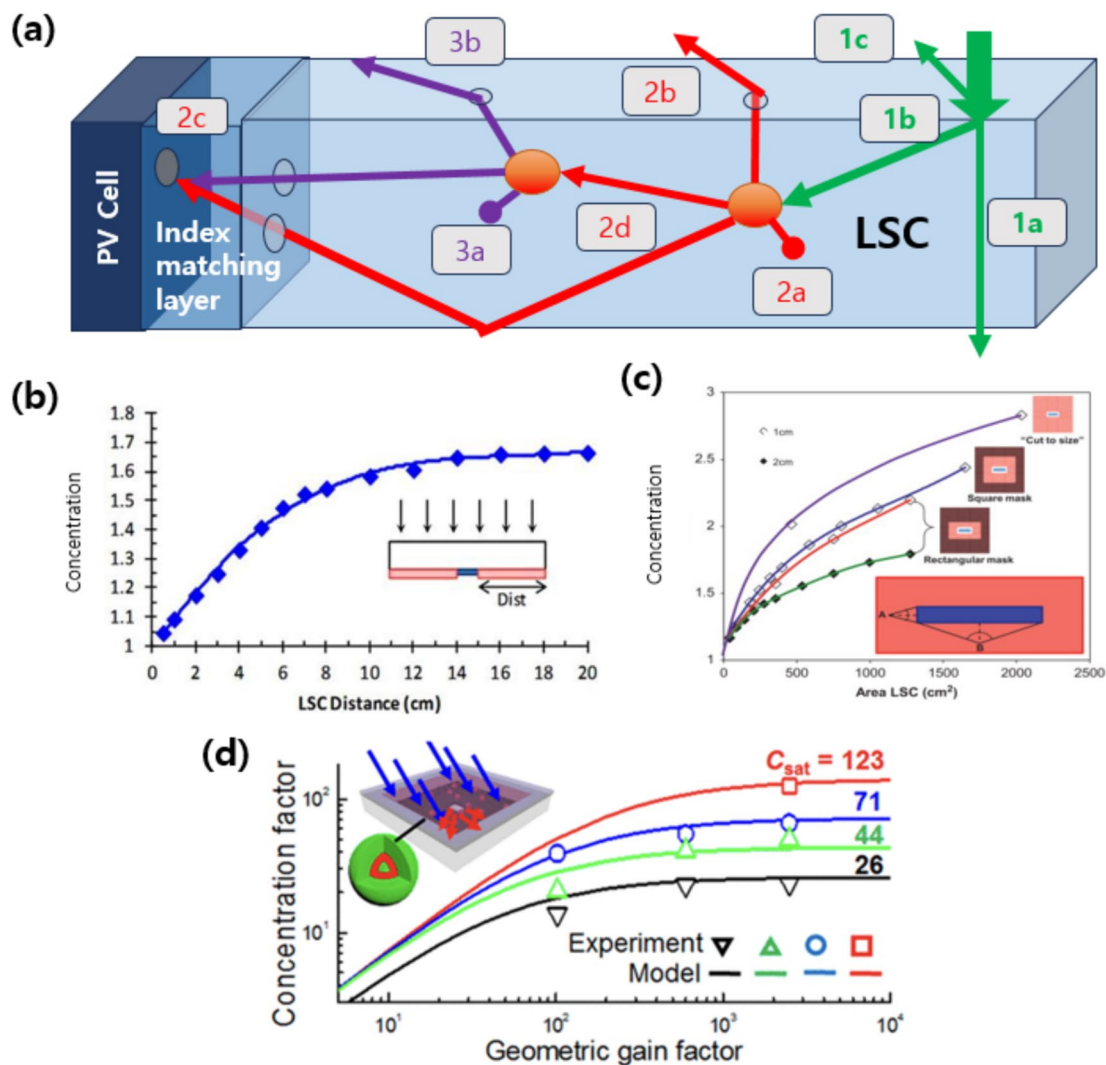
Fig. 2 **a** Working principle and loss mechanism of the LSC. **b** Theoretically calculated relative C of a PV cell (width of 2 cm) as a function of the length of the LSC. Here, the normal incident light irradiates the front side of LSC, where the PV is located in the middle of LSC (Reproduced with permission [46], Copyright 2013, AIP publishing), **c** C of the LSC with different types of masking and cut-to-size techniques. While the enlarged LSC area leads to higher C, the C is saturated in all cases regardless of the shape of the LSC. (Reprinted with permission [47], Copyright 2013, Elsevier) **d** C of LSC enveloped by specular (blue) and diffusive reflector (green), compared to without a reflector (black). Additional improvement is achieved by incorporating a selective reflector at the front side of LSC (red). However, the C is also saturated despite the introduction of reflectors to the LSC (Reprinted with permission [48], Copyright 2018, American Chemical Society.)

essential, along with exploring methods to reduce photon escape and reabsorption losses. Most recent studies focus on developing highly efficient LSCs by reducing these losses.

Despite the recent progress, the concentration of LSC (C) does not increase proportionally to its geometrical gain (G), which is defined as the ratio of the front collection area of the LSC (A_{LSC}) to the edge and area of the PVs (A_{PV}), and saturates at a specific value. Previous works indicated that the C of LSC increases proportionally to the G when the size of LSC is small. However, beyond a certain length, photon loss during waveguiding increased due to an increased likelihood of re-absorption and escape.

Consequently, the theoretically and empirically attainable C plateaued at certain values [46]. The introduction of an optimized configuration of LSC and selective reflector might increase the C of LSC, but the saturation of C was also observed in the LSC having different dimensions [47] and selective reflectors [48].

The theoretical analysis indicates that the performance of LSCs is constrained by the loss from re-absorption and poor η_{trap} [49–51]. Typically, the power conversion efficiency of PVs attached to LSC ($\eta_{LSC,PV}$) is defined as follows:

$$\eta_{LSC,PV} = \eta_{PV} \times \eta_{opt} \qquad (1)$$

where η_{pv} represents the efficiency of the PVs, while η_{opt} signifies the overall optical efficiency of the LSC, indicating the ratio between incident photons to waveguided photons reaching the PVs. Consider an LSC with dimensions (width: W, Length: L, and thickness: d) depicted in Fig. 3(a), the C of the LSC, calculated as the ratio between total incident photon flux in the front (Φ_I) and at the edge of the LSC (Φ'_2, Φ''_2), is determined as the product of η_{opt} and G

$$C = \frac{(\Phi'_2 + \Phi''_2)/A_{PV}}{\Phi_1/A_{LSC}} = \frac{\Phi'_2 + \Phi''_2}{\Phi_1} \times \frac{A_{PV}}{A_{LSC}} = \eta_{opt} \times G \quad (2)$$

Assuming η_{opt} remains constant regardless of the LSC dimension, the C will increase proportionally to G. However, beyond a certain value, further enhancement of C becomes unfeasible, due to the negative correlation between η_{opt} and G as shown in Fig. 2.

As η_{opt} encompasses all optical losses, including photon annihilation during re-emission, scattering, and re-absorption within the luminophores, as well as reflection, transmission, and other optical losses, it can be expressed as follows:

$$\eta_{opt} = (1 - R) \times \eta_{trap} \times \eta_{abs} \times \eta_{PLQY} \times \eta_{RA} \qquad (3)$$

Here, the R represents reflection at the waveguide surface. η_{trap} denotes the likelihood of being trapped within the LSC by internal total reflection, approximately ~ 0.75. Moreover, η_{abs} signifies the efficiency of light absorption of the luminophore, calculated as $\eta_{abs} = (1 - e^{-\alpha(\lambda)d})$, where $\alpha(\lambda)$ represent the absorption coefficient of luminophores at the wavelength of λ. Lastly, η_{RA} represents the efficiency of re-absorption due to inherent multiple reabsorptions and re-emissions during the waveguide to PVs. Optimal η_{RA} is attained when the luminophore's absorption coefficient α_1 at the wavelength of incident light (λ_1) is substantially higher than the absorption coefficient α_2 at the emission center wavelength of re-emission (λ_2) (Fig. 3(b)). As η_{RA} negatively correlates with the G ($=L/d$), η_{RA} is expressed as follows:
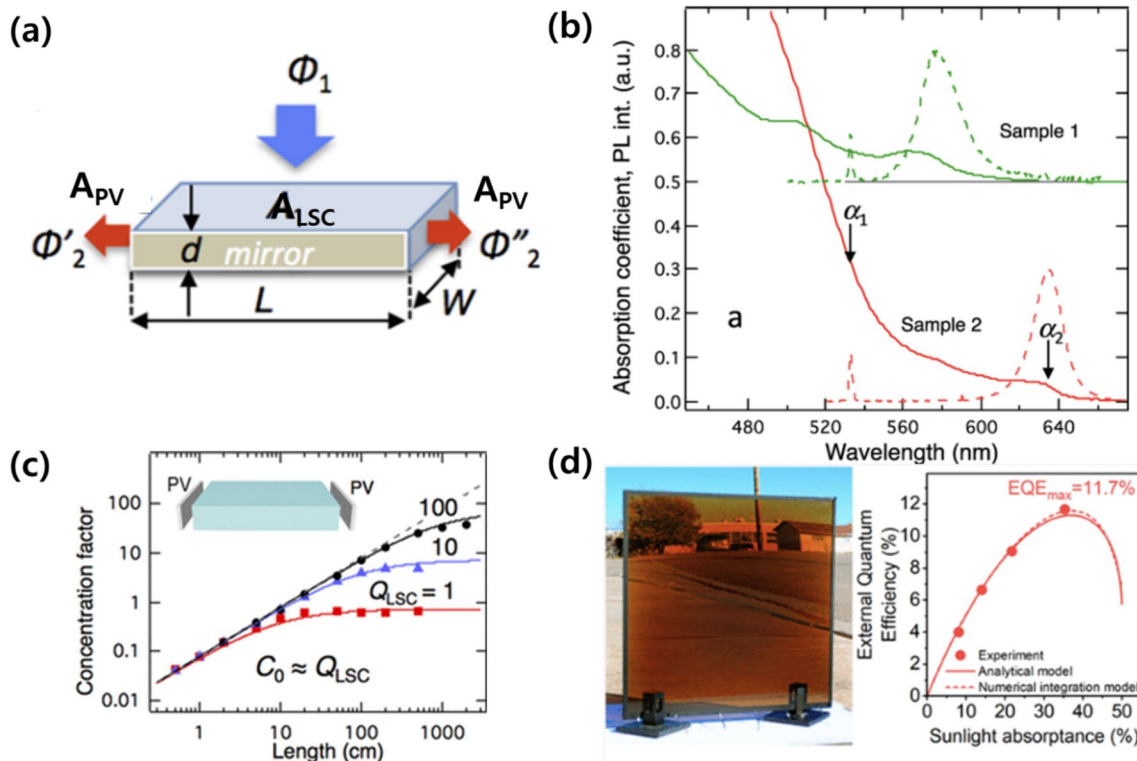
Fig. 3 **a** A schematic of LSC. A portion of the incident flux (Φ_1) impinges the front surface (A_{LSC}) of the LSC. Some of the photons are absorbed by the luminophores and re-emitted toward edge-mounted PVs (output flux of Φ'_2 and Φ''_2), **b** Absorption and emission spectra of luminophore. The α_1 and α_2 are the absorption coefficients of luminophores at the absorption and re-emission peak wavelengths, respectively. Sample 1 (green) shows a higher α_2 compared to sample 2 (red). **c** The relationship between LSC length and C with luminophores having different Q_{LSC}s. (Reprinted with permission [50], Copyright 2016, American Chemical Society) (**d**) External quantum efficiency of LSC as a function of sunlight absorptance under outdoor conditions (Reprinted with permission [49], Copyright 2022, American Chemical Society.)

$$\eta_{RA} \approx 1 / \left(1 + \alpha_2 \beta L \left(1 - \eta_{trap} \eta_{PLQY}\right)\right) \tag{4}$$

where the correction factor for optical loss is denoted by β. For planar LSC, the C of LSC with a structure shown in Fig. 3(a) is defined as follows:

$$C = \eta_{opt} \times G = (1-R) \frac{\left(1 - e^{-<\alpha_1>d}\right) \eta_{trap} \eta_{PLQY}}{1 + <\alpha_2> \beta L \left(1 - \eta_{trap} \eta_{PLQY}\right)} g \tag{5}$$

Here, $<\alpha_1>$ and $<\alpha_2>$ denote the average absorption coefficients across the absorption and emission spectrum of luminophore, respectively. Equation (5) reveals the trade-off relationship between G (=L/d) and η_{opt} caused by re-absorption losses. As a result, the theoretically attainable maximum η_{opt} from 1000 cm^2-sized LSC is below 10% [52]. Similar results, significant reduction of η_{opt}, have been reported in large-sized LSC (> 300 cm^2) [53–56].

To overcome the trade-off relationship between G and η_{opt}, three strategies have been suggested. According to Eq. (5), an ideal luminophore should possess a high η_{PLQY} to re-emit the light with small losses and a high $<\alpha_1>$ to effectively absorb incident light. Additionally, a low $<\alpha_2>$, indicating minimal overlap between the absorption and emission spectrum of luminophore, is essential. As shown in Fig. 3(c), the quality factor (Q_{LSC}), defined as the ratio between $<\alpha_1>$ and $<\alpha_2>$, plays a vital role in limiting the attainable C in the LSC [50, 57, 58]. Furthermore, optimizing the luminophore concentration is necessary due to a trade-off relationship between $<\alpha_1>$ and $<\alpha_2>$, theoretical simulation based on Eq. (5) and validated through experiment (See Fig. 3(d)) [49, 59]. Lastly, a high η_{trap} enhances the C by entrapping re-emitted photons within the LSC. Considering these factors that limit the performance of LSCs, the most of research has focused on developing reabsorption-free luminophores with high η_{PLQY} and improving η_{trap}. The detailed progress in each aspect will be discussed next chapters.

Development Of Luminophore for Efficient LSC

As properties of the luminophore influence the absorption of incident light, re-emission efficiency, and re-absorption in the LSC, the development of luminophore contributes to unlocking the full potential of LSCs. The stoke shift of representative luminophores and efficiency of LSC with them are summarized in the Table 1. In the initial stages of LSC development, most luminophores were organic dyes, whose advantages included an easy synthesis process using earth-abundant materials. Among many suggested organic materials, perylene-based organic dye (Fig. 4(a)), Lumogen F Red305 (BASF), emerges as a highly promising candidate for LSC due to its high η_{PLQY} and $<\alpha_1>$ [66–68]. An LSC incorporating Lumogen F Red 305 and GaAs solar cell achieved an $\eta_{LSC,PV}$ of 7.1%, showing the possibility of large-sized LSC (5 ×5 cm^2) [69]. Nevertheless, the extensive overlap between emission and absorption spectra in organic dyes limits the performance and size of LSC due to increased re-absorption losses. Hence, recent research endeavors focused on energy transfer within organic molecules to expand the Stokes shift. X. Li et al proposed aggregation-induced emission molecules, whose η_{PLQY} is close to unity, and Stokes shift reaches 0.59 eV [37]. The incorporation of aggregation-induced emission molecules suppressed reabsorption losses, enabling the enlargement of LSC dimensions. They achieved an $\eta_{LSC,PV}$ of 1.4% in a 100 cm^2-sized LSC with a visible transmittance reaching 87%. Additionally, several research groups demonstrated

Table 1 List of some of the representative luminophores, their stoke shift, LSC size, empirically achieved efficiency, and references

Luminophore		Stoke shift (nm)	Size (cm^2)	$\eta_{LSC,PV}$	References
Organic molecules	Red 305	38 nm	25	7.1%	[69]
	aggregation-induced molecules (TPA-BT)	129 nm	100	1.4% (Transparent)	[37]
	aggregation-induced molecules (PFPBNT)	120 nm	1600	3.5%	[70]
Quantum dot	CdSe/CdS	> 120 nm	> 20 cm (1 axis)	10.2% (η_{OPT})	[74]
	Mn^{2+-}doped ZnSe/ZnS	> 150 nm	20	37% (η_{OPT})	[62]
	InP/ZnSe	~ 200 nm	25	2%	[63]
	CuInS$_2$/ZnS	> 150 nm	4.84	8.7%	[103]
			232	3.6%	[104]
	Ag(In,Ga)S$_2$/AgGaS$_2$	~ 50 nm	50	9.4% (η_{OPT})	[107]
	Si	150 nm	144	2.8%	[115]
	Carbon dot	98 nm	100	2.7%	[118]
	Perovskite QDs (HA$_2$MA$_{n-1}$Pb$_n$Br$_{3n+1}$)	50 nm	100	26% (η_{OPT}) 0.87%	[121]
	Perovskite QDs (Cs$_4$PbBr$_6$)	196 nm	100	2.7%	[113]

Fig. 4 Representative lumino-phores for LSC: **a** perylene-based organic dye (Lumogen Red 305, Reprinted with permission [60], Copyright 2018, Wiley–VCH), **b** CdSe/CdS core/shell QDs (Reprinted with permission [61], Copyright 2016, American Chemical Society), **c** heavy metal (Mn^{2+})-doped ZnSe QDs (Reprinted with permission [62], Copyright 2014, American Chemical Society), **d** eco-friendly InP/ZnS QDs (Reprinted with permission [63], Copyright 2023, American Chemical Society) and **d** surface-modified carbon dot (Reprinted with permission [64], Copyright 2017, Elsevier). **e** absorption (green) and emission (green) spectrum of representative luminophores (Reprinted with permission [65], Copyright 2023, Elsevier.)
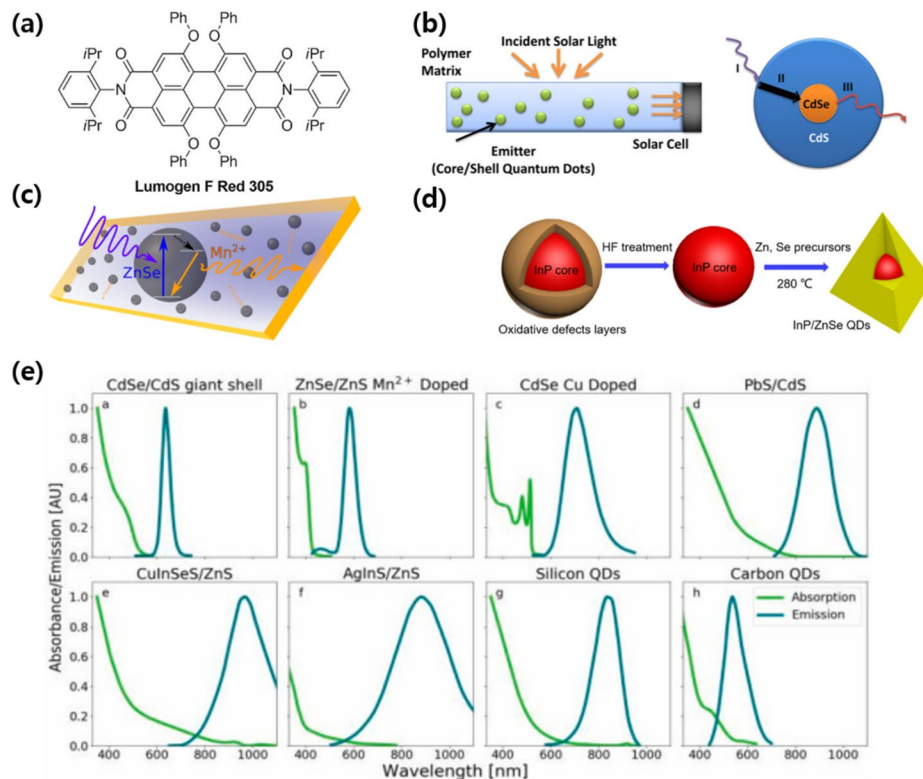
highly efficient LSCs by integrating aggregation-induced fluorinated emitters, benzothiadiazole, and benzothiophene derivatives with Stokes shift exceeding 0.5 eV [70–72]. Suppressing re-absorption losses in large LSCs (1,600 cm^2) yielded an $\eta_{LSC,PV}$ exceeding 3%, showing the possibility of scaling up of LSCs with organic luminophores. Considering lifetime of window or building envelope, the LSC should withstand harsh outdoor conditions at least 10 years. However, poor photo and thermal stability of organic-based luminophore is a key challenge for the commercialization of LSC with them. The selection of suitable host material for protecting organic luminophores from heat and UV light will be a solution for them [37].

As validated in the LSC with organic luminophores and theoretical calculation, the Stokes shift plays an important role in determining the maximum achievable $\eta_{LSC,PV}$ of LSC. In comparison to other luminophores, the core/shell QDs maximize the Stokes shift by employing different materials for the core and shell, respectively. Consequently, the core/shell QD-based LSCs have been intensively studied to tackle re-absorption challenges (Fig. 4(b)). Initially proposed as a promising luminophore candidate for LSCs in early 2010 [31, 61, 73–75], core/shell QDs possess the capability to disperse into a polymer matrix with chemical robustness, thereby mitigating luminescent quenching due to radicals or photooxidation [31]. Furthermore, the thick shell of QDs impedes exciton energy transfer between QDs and the polymer layer, leading to reduced luminescence

quenching [76, 77]. The reduced re-absorption coupled with the maintenance of high η_{PLQY} in core/shell QDs allowed us to demonstrate the large-sized LSCs. F. Meinardi et al. proposed Stokes shift-engineered CdSe/CdS QDs to enable highly efficient LSCs with minimized reabsorption losses. Featuring a giant CdS shell, ~ 50 times larger than the core, these QDs absorb blue and green light, while the CdSe core emits red light (with a peak wavelength of 640 nm), as depicted in Fig. 4(e) [74]. The reduced overlap between absorption and emission spectra allowed them to scale up the size of the LSC up to 20 cm and achieve a C of 4.4. The result indicates the significant potential of Stokes shift-engineered QDs for large-area LSCs. Furthermore, systematic research has revealed that increasing the shell thickness results in a consistent reduction in reabsorption. In CdSe/CdS QDs, the QDs with a thick shell, comprising approximately 14 monolayers of CdS, exhibited a 45-fold decrease in re-absorption losses compared to QDs with only a CdSe core. Additionally, an improved synthesis method maintained an η_{PLQY} of 86% in solution, even for QDs with the thickest shell. Monte Carlo simulations have identified that reabsorption-free LSCs can be achieved using these giant core/shell QDs [61].

Expanding the Stokes shift of luminophores involves doping heavy metals into QDs (Fig. 4(c) and (e)). In metal-doped QDs, their emission spectrum experiences a red shift due to the intra-gap states of dopant ions compared to those of undoped ones [78–81]. Conversely, the absorption

characteristics of the shell remain unchanged, thereby contributing to an expanded Stokes shift. Transition-metal ions, such as Mn [82, 83] and Cu [84, 85] ions, are often used as dopants to induce red shifting of emission spectra in QDs. Consequently, metal-doped QDs have been integrated into LSCs as luminophores. For instance, Mn^{2+}-doped ZnSe/ZnS QDs selectively absorb UV and blue light, while emitting yellow and orange light through the inter-gap state of ZnSe by doping Mn^{2+}(Fig. 4(c)). With the expanded Stokes shift of Mn^{2+}-doped ZnSe/ZnS QDs suppressing the reabsorption of emitted photons, the C of 15.6 and η_{opt} of 37% were achieved in a large-sized LSC (dimension of $25 \times 75 \times 0.42$ mm) [62]. Moreover, by confining the absorption spectrum from UV to deep blue, the proposed LSC emerges as a strong candidate for replacing conventional windows with energy-harvesting ones. In another study, doping Cu into CdSe colloidal quantum wells (CQWs) not only expanded the Stokes shift by tuning defect-induced luminescent emissions but also achieved a near-unity η_{PLQY} ($\sim$97%) [85]. Furthermore, Cu doping resulted in increased absorption cross sections and inherently stepped absorption profiles, both of which are advantageous for LSCs. Leveraging these outstanding characteristics, doped CQWs proved to be excellent candidates for LSCs.

Despite the excellent optical properties of Cd-containing QDs for LSC, they are hindered by environmental concerns stemming from the toxicity of Cd and limited absorption resulting from a wide band gap. As small amount of Cd leaching from QDs is very critical to human body, the Cd-based QD is reluctant to use as an energy-generating window. In addition, the exposure of Cd-based QDs to living animals and plants results in increased concentration of Cd in their body [86]. Consequently, emerging binary, eco-benign QDs have garnered significant attention for their excellent optical properties. For example, Ag_2S [87], Ag_2Se [88], CuS [89], CuSe [90], and InP [26, 63, 91] exhibit their potential in practical QD-based optoelectronic devices and imaging systems. Altering the stoichiometry of QDs and introducing an additional shell layer to eliminate residual precursors or defect sites have significantly enhanced η_{PLQY} of binary QDs [92–94]. However, LSCs with core/shell InP/ZnS exhibited low η_{opt}, primarily attributed to a strong overlap between emission and absorption spectra [95]. Furthermore, oxide and defect sites present on the InP core during its synthesis serve as annihilation centers of photogenerated excitons, which decrease η_{PLQY}. These challenges can be mitigated by incorporating a thicker shell layer with precursor control during QD growth. The increased thickness of the ZnS shell layer maximizes Stokes shift by separating the absorption of incident light through the thick shell and the emission of absorbed photons via effective energy transfer [63]. Additionally, the elimination of oxides on the InP core surface prior to shell growth has been demonstrated to

enhance the η_{PLQY} of pyramidal InP/ZnSe QDs, as shown in Fig. 4(d). Moreover, the introduction of ZnO shell [26], doping organic molecule (rhodamine 101) [96], and heavy metal (Cu) [91] to InP QDs pave the way to increase the Stokes shift, thereby contributing to suppressing parasitic absorption issues in LSCs with InP QDs. Furthermore, the engineering of precursors or additional buffer layers (ZnS) aids in eliminating defect states, thus boosting η_{PLQY} [92, 97]. Furthermore, through ligand exchange, the dispersion of InP/ZnS QDs in a polymer layer is achieved, thereby reducing aggregation [95]. While the efficiency of InP/ZnSe-based LSC remains relatively low efficiency and complicated synthesis process compared to the CdSe-based QDs at present, its environmentally friendly feature makes it a strong candidate for LSC luminophores. Besides, the rapid growth of the InP QDs market within the display industry is driving efforts to further reduce the fabrication costs of LSCs using these materials [98, 99].

Ternary QDs, including $CuInS_2$ (CIS), $CuInSe_2$ (CISe), and their alloys ($CuInSe_xS_{2-x}$), represent another group of non-toxic luminophores with large Stokes shifts. Unlike III–V and II–VI QDs, ternary QDs exhibit a much larger Stokes shift owing to their inter-energy state [100]. Consequently, ternary QDs do not require core/shell heterostructures, making them ideal for mass production through high-throughput solution-phase synthesis using inexpensive precursors without involving heavy metals [101]. These ternary QDs exhibit significant absorption cross sections, tunable spectra, and absorption spectra with nearly featureless profiles extending over the entire visible range, rendering them well-suited for harvesting solar radiation [102]. Additionally, the emission spectrum of ternary QDs aligns with the bandgap of widely used crystalline Si PVs (near IR region). Utilizing colorless and reabsorption-free CIS QD-based LSC meets the criteria for window applications, demonstrating high η_{PLQY} ($>$90%) and η_{opt}. One of the most outstanding performances was achieved with $CuInS_2$/ZnS core/shell QDs with a η_{PLQY} of $\sim$81% and a Stokes shift of over 150 nm, resulting in a $\eta_{LSC,PV}$ of 8.7% when integrated with c-Si PV [103]. At the large-sized LSC (152.4×152.4 mm) with optimized $CuInS_2$/ZnS QDs and optical structure, $\eta_{LSC,PV}$ of 3.6% was achieved, exhibiting economically viability of LSC [104]. Another proposed approach involves replacing Cu with Ag for highly efficient LSCs [59]. QDs composed of silver indium gallium sulfide (Ag(In, Ga)S_2) have garnered increasing attention due to their narrow emission bandwidth and high absorption cross section [105, 106]. However, their relatively poor η_{PLQY} hampers their potential application in optoelectronic devices. Incorporating an $AgGaS_2$ shell layer onto Ag(In, Ga)S_2 QDs significantly enhances their η_{PLQY}, nearly achieving unity [107]. This enhancement renders them directly applicable in practical settings, such as displays and LSCs. Utilizing

Ag(In, Ga)S$_2$/AgGaS$_2$ core/shell QDs in LSCs successfully demonstrated higher efficiency (η_{opt} of 9.4%) while reducing the amount of luminophores. Due to the reduced concentration of luminophores and minimized re-absorption losses, cost-effective and large-sized LSCs can be achieved using Ag(In, Ga)S$_2$/AgGaS$_2$ core/shell QDs.

However, the η_{PLQY} of previously suggested QDs, including Cd-based, non-Cd-based, binary, and ternary QDs, reduces significantly at polymer matrix, posing a major challenge commercialization of LSC. While the state-of-the-art η_{PLQY} of QD is nearly unity in the solution, a reduction in η_{PLQY} is inevitable in polymer matrices due to their poor surface passivation and aggregation [108]. Proper selection of host matrix materials and effective QD dispersion methods are essential to unlocking their full potential as luminophores for LSCs. Additionally, the lack of long-term stability testing for QD-based LSCs raises concerns about their feasibility. Introducing an additional silica shell to protect QDs from UV radiation and humidity has provided stable LSC performance under heat and UV exposure [109]. Finally, methods to produce a thin luminophore film within the waveguide matrix, such as spray and bar-coating techniques, are required. Overcoming these issues is crucial for improving the efficiency, stability, and installation methods of QD-based LSCs.

Lastly, earth-abundant Si, carbon [110, 111], and perovskite QDs [112–114] have the potential to reshape the spectrum of incident light and direct it toward edge-mounted PVs. These materials are biocompatible and environmentally benign, offering an alternative to toxic luminophores. Si QDs, characterized by an indirect band gap, exhibit a significant Stokes shift and long-lived luminescence (hundreds of microseconds). The reduced re-absorption losses associated with Si QDs enable the attainment of η_{opt} of 2.8% in LSCs when employing a thick waveguide plate and a thin film of Si QDs, which are comparable to other green-colored QDs [115]. However, their drawback lies in a reduced η_{PLQY} (below 50%), attributed to the activation of the additional non-radiative pathways and surface oxidation. Furthermore, scattering effects due to the high refractive index of Si QD must be addressed. To address these challenges, Si QDs were incorporated into poly(methyl methacrylate) nano-composites, which curtails QD aggregation in active LSC films, thereby mitigating non-radiative effects and scattering [116]. Meanwhile, carbon QDs are easily processed organic colloidal nanocrystals from inexpensive precursors, which is advantage for mass production with reduced cost. Although carbon dots are often categorized as QDs, their properties lie between organic dyes and other inorganic QDs, rendering them an appealing alternative expected to overcome significant luminophore concerns, such as toxicity and stability [64]. Their rich surface groups (such as amino, carboxyl, and hydroxyl groups) render them more soluble in various non-toxic solvents, including water, thus suitable for the development of eco-friendly LSCs. Like other QDs, they also exhibit tunable optical properties and high η_{PLQY} [117]. The $\eta_{LSC,PV}$ of 3.0% was successfully achieved in the LSC (25 cm^2) with produced via the space-confined vacuum-heating approach [118]. However, a drawback of carbon QDs is their relatively small Stokes shift, which limits the efficiency of LSCs due to re-absorption losses (see Fig. 4(e)) [118]. As a result, the significant drop of $\eta_{LSC,PV}$ (2.2%) was observed in the large-sized LSC (225 cm^2) with carbon dot. Moreover, carbon dot shows relative poor stability under UV light. As the role of LSC is to down-shifting incident light, containing UV and blue light, the photostability of carbon dot should be overcome for acting as luminophores in LSCs. Similar to carbon QDs, perovskite QDs can be synthesized using earth-abundant precursors at low temperatures. The large Stokes shift observed in heavy metal-doped perovskite QDs allows for the development of re-absorption-free LSCs, facilitating the enlargement of their size [57, 119, 120]. In addition, perovskite QDs absorb a broad range of solar spectrum, contributing to increased $\eta_{LSC,PV}$. As the different optical properties of perovskite QDs are easily achieved by modifying the chemical formula, perovskite QDs are considered as ideal luminophore for LSC. The absorption and emission spectrum of perovskite QDs can be tailored for specific photovoltaic cells, which can maximize the efficiency of LSC [113, 121]. However, their poor stability against humidity, oxygen, and light irradiation impedes their widespread use as luminophores in LSCs [122, 123]. Especially, the poor performance of perovskite QDs under UV and blue light has been criticized [124, 125]. Moreover, relative poor η_{PLQY} of perovskite QDs at polymer matrix should be overcame [113, 122, 123]. If these drawbacks are addressed, these alternative QDs stand to gain a competitive advantage as luminophores.

Device Structure Engineering for Efficient QD-Based LSC

Intensive efforts in device structure engineering have been undertaken to fully harness the potential of luminophores in the LSCs, leading to improved performance. Reabsorption losses can significantly reduce η_{opt}. One effective method for mitigating reabsorption losses involves enlarging the Stokes shift by incorporating Förster resonance energy transfer (FRET) between two different luminophores, as shown in Fig. 5(a) [126, 133, 134]. In FRET systems, donor luminophores absorb incident light and transfer energy to an emitter whose bandgap is smaller than that of the donor. When the concentration of donors is significantly higher than that of emitters, the overall absorption spectrum of the LSC is
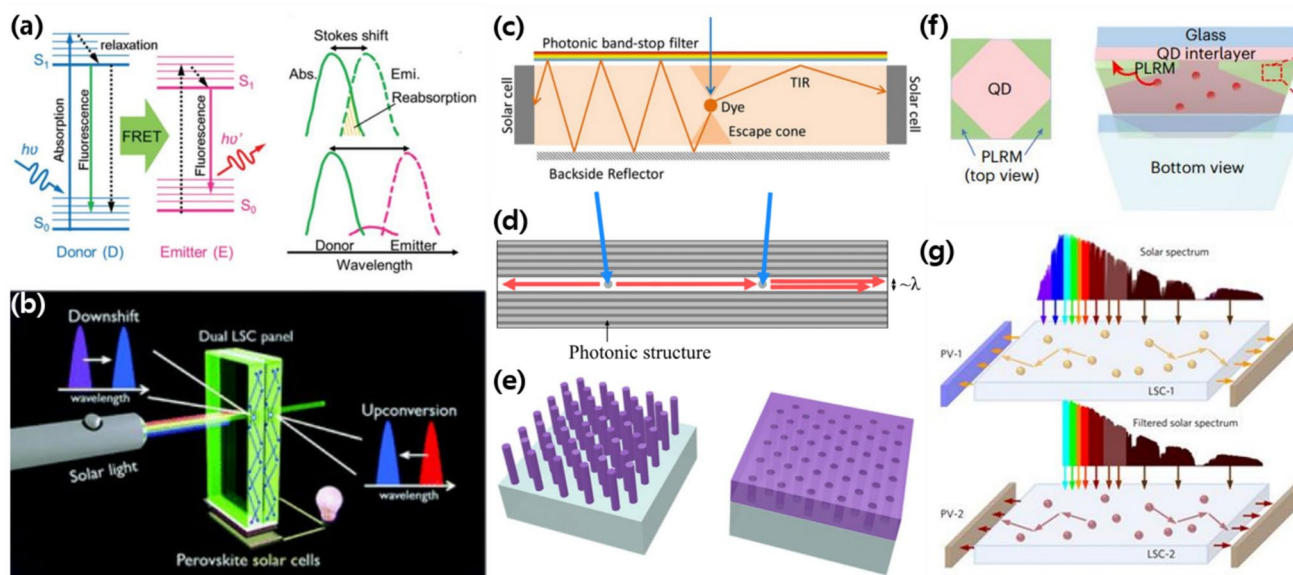
Fig. 5 a Schematic of FRET in luminophore. The FRET helps minimize the overlap between the absorption and emission spectrum. (Reprinted with permission [126], Copyright 2022, Wiley–VCH), **b** Dual-band LSC with down and up-conversion luminophores (Reprinted with permission [127], Copyright 2020, The Royal Society of Chemistry). **c** A band-stop filter for selective reflection enhances photon recycling by decreasing escaping photons in LSC (Reprinted with permission [128], Copyright 2016, American Chemical Society), **d** An LSC consists of luminophores embedded in a photonic crystal. (Reprinted with permission [129], Copyright 2012, Optical Society of America.), **e** Periodic rod and hole arrays–based photonic crystals made of hydrogenated amorphous silicon carbide for waveguiding re-emitted light from CdSe/CdS QDs. (Reprinted with permission [130], Copyright 2020, American Chemical Society.), **f** Diagram of an LSC with patterned low-refractive-index medium for minimizing optical losses during the waveguiding. (Reprinted with permission [131], Copyright 2024, Springer Nature.), **g** Tandem-structured LSC composed of different layers mixed with two different luminophores: Mn^{2+}-doped $Cd_xZn_{1-x}S$ QDs (top) and CIS QDs (bottom). (Reprinted with permission [132], Copyright 2018, Springer Nature.)

primarily determined by donor characteristics. Conversely, the emission spectrum of the FRET system originates from the emitter, leading to an enhanced effective Stokes shift. To facilitate effective energy transfer between donor and emitter, proximity between them is essential. As a result, the FRET system primarily comprises organic luminophores (emitter) attached to the surface of inorganic QDs (donor). A luminophore-assisted LSC based on FRET was demonstrated on a flat plastic substrate by applying a dye blend film using doctor-blading. Here, the organic heteropentacyclic compound Alexa Fluor 546 was used as an emitter, receiving energy from CdSe(core)–ZnS(shell) QDs. The ray-tracing simulation indicated that embedding FRET-based luminophores in the LSC achieves a maximum η_{opt} of 75.1%. This efficiency is 215.5% higher than that of an LSC with only QDs [135].

Another possible energy transfer mechanism for enhancing the performance of LSCs is up-conversion [127, 136, 137]. A primary challenge with conventional luminophores is their limited absorption spectrum, leading to comparatively weak light harvesting compared to direct PVs. Combining a down-shifting luminophore with an up-conversion molecule can broaden the spectral range for sunlight harvesting. Specifically, up-conversion molecules facilitate the conversion of penetrating low-energy photons to ones with higher energy that can be converted into electricity. Integrating up-converters with QDs enabled the development of a dual-band LSC, as shown in Fig. 5(b) [51]. Incorporating up-conversion into a dual-band harvesting LSC, which consists of down- and up-converting materials for luminophores integrated with perovskite PV cells, yielded an average visible transmittance of 82% and an $\eta_{LSC,PV}$ of 7.53%. Additionally, the up-conversion of unharvested photons through nitrogen-doped graphene QDs enhanced LSC efficiency [136]. If up-conversion efficiency is improved, the improved efficiency of LSC will be achieved by extending the absorption spectra of luminphores. Thus, the combination of down- and up-converting molecules with luminophores contributes to improving $\eta_{LSC,PV}$ by broadening the absorption spectrum.

Incorporating selective reflectors into LSC suppresses the optical loss. A significant factor limiting η_{opt} of large-sized LSCs is escape cone loss, primarily due to scattering and reabsorption. Applying a band-stop filter to the front side of the LSC can enhance efficiency. This filter reflects re-emitted photons while transmitting photons in the range of the absorption spectrum of luminophore, thus reducing escaping photons and increasing $\eta_{LSC,PV}$, as shown in Fig. 5(c). The selective reflector demonstrates high transmittance in the

absorption spectrum of the luminophore while exhibiting extremely high reflectivity in its emission spectrum. Consequently, this selective reflector enhances η_{opt} of the LSC by recycling re-emitted photons within the escape cone [128]. Distributed Bragg reflectors (DBRs), comprising a stack of multiple dielectric layers, stand out as one of the most widely used selective reflectors applied to the front side of LSC. The DBR permits light within the absorption band to pass through with minimal losses while reflecting re-emitted light. Consequently, a greater number of photons become trapped within the LSC, leading to an increased photon yield directed toward PVs. For instance, in an LSC, whose dimension is $50 \times 100 \times 5$mm, the incorporation of a DBR onto its front side increased $\eta_{LSC,PV}$ from 2.6% to 3.1% [138]. Additionally, surrounding the other edges of LSC with a perfect reflector enhances the waveguiding of re-emitted light. The combination of DBR and diffusive reflector resulted in a 23% improvement in the η_{opt} of the LSC compared to one without DBR [128]. A similar outcome was observed in an LSC enclosed by a selective reflector on the front side and a specular reflector (metallic reflective film) on the backside and other edges, achieving a *C* exceeding 120 at the specific wavelength of the PL spectrum [48]. Notably, the specular reflector proved more efficient in reducing optical loss compared to the diffusive reflector by maintaining the trajectory of re-emitted light during reflection. These approach allows us to keep η_{opt} in large-sized LSC, facilitating the scaling up of LSCs.

To achieve the ultimate *C* of LSCs, a photonic crystal was also applied to the LSC, as illustrated in Fig. 5(d). This configuration featured a photonic crystal integrated into the LSC, with luminophores located in the photonic crystal [139]. By confining the emitted light's trajectory to the plane direction, the photonic crystal shortened the path of re-emitted light to PV cells, reducing the likelihood of re-absorption by other luminophores. Consequently, the η_{opt} was significantly enhanced in CdS/CdSe QD-based LSC enclosed by a stack of Si_3N_4 and SiO_2. It showed a 40% increase in η_{opt} and a considerable reduction in reabsorption losses. Furthermore, the rod and the hole array–based photonic crystals, composed of hydrogenated amorphous silicon carbide, were integrated into the LSC with CdSe/CdS QDs, as depicted in Fig. 5(e). The 3D structured photonic crystal effectively recycled photons within the escape cone, leading to a light trapping efficiency of 92% and C of 100 in the LSC [130].

While DBR and photonic crystals offer improved η_{opt} by recycling escaping photons, their fabrication process involves precise thickness control via vacuum deposition and a complicated lithography process. However, due to their high-cost fabrication methods, the feasible application area for DBR and photonic crystals remains limited. Moreover, these optical structures are not desirable for large-sized LSC

due to the cost. Consequently, many research groups focused on replacing them with simple processed selective reflectors, with polymer dispersed liquid crystal (PDLC) being one of the alternative reflectors. PDLC consists of a mixture of liquid crystal and polymer layers, with its transmittance controlled by an applied voltage. Incorporating a PDLC-based smart window into the LSC resulted in η_{opt} and $\eta_{LSC,PV}$ values of 4.52% and 2.49%, respectively, which are 1.7 times higher than those achieved by LSCs without PDLC. With PDLC acting as an on–off switchable smart window, trapping escaping photons within the LSC, the LSC with PDLC holds promise as a candidate for zero-energy building windows by blocking unwanted solar irradiance and maximizing the efficiency of LSC [140]. Cholesteric liquid crystals (CLCs) integrated with graded-index reflectors also function as selective reflectors for LSCs. The reflection band of CLCs can be modified by adjusting the layer thickness, enabling selective reflection through thickness-controlled CLCs. Moreover, the graded refractive index facilitates the transfer of escaping photons to edge-mounted PVs. By incorporating CLCs into LSCs, the η_{opt} of LSCs saw a 12% increase with a periodic CLS reflector [141]. Recently, there has been significant interest in light-guiding media for LSCs due to their excellent waveguiding properties. Figure 5(f) illustrates QD-based LSCs featuring patterned low-refractive-index medium (PLRM), which offers non-decaying paths for re-emitted light. The PLRM comprises hollow silica nanoparticles, whose vacant inner pores contribute to a lower refractive index. Consequently, more re-emitted light is captured by the PVs, leading to reduced losses from escaping, scattering, and re-absorption. Hence, LSCs incorporating PLRM and reflectors achieved an $\eta_{LSC,PV}$ of 7.6% for an LSC size of 100 cm^2 [131]. The proposed selective reflectors and waveguiding structures enable the expansion of LSC size, a crucial step toward their potential use in window replacement. Further research about them will provide better waveguide efficiency with reduced cost.

Another strategy to maximize *C* of LSCs involves utilizing a tandem structure, composed of more than two waveguide plates doped with different luminophores. The narrow absorption spectrum of luminophore often restricts the $\eta_{LSC,PV}$ of a single LSC. Consequently, many research groups are exploring the possibility of improvement in $\eta_{LSC,PV}$ by applying additional emitters. As illustrated in Fig. 5(g), tandem-structured LSCs, comprising two different layers mixed with different luminophores, absorb a broad range of solar radiation using spatially separated luminophores. The top LSC covers high-energy photons, while the bottom LSC absorbs photons penetrating the top LSC. Besides, the re-absorption losses will be diminished by spatially separating luminophores [142]. K. Wu et al. utilized Mn^{2+}–doped $Cd_xZn_{1-x}S$ QDs for the top layer of

tandem-structured LSC, with CIS QDs serving as secondary luminophores. The η_{opt} of tandem-structured LSC was 52% higher than that of a single LSC with only one luminophore [132]. Similar results were also obtained in a tandem LSC comprising red and green carbon dots. The combination of two different dots at tandem-structured LSC leads to a 20% improvement in the $\eta_{LSC,PV}$, compared to a single LSC [143]. The tandem structure LSC with $CsPb(Cl_xBr_{1-x})_3$ QDs and C-dot layer also demonstrated 27% improvement in $\eta_{LSC,PV}$ [112]. Moreover, the tandem structure contributes to enhancing the stability of LSCs by reducing exposure to high-energy photons. G. Liu et al. proposed a tandem-structured LSC incorporating CdSe/CdS QDs and carbon dots. By doping carbon dots into the top plate, they efficiently absorb high-energy photons, waveguiding them into the PVs. This lowers the probability of CdSe/CdS QDs located at the bottom plate being irradiated by UV light. Consequently, the long-term photostability of the LSC significantly improved. After 70 h of UV illumination, it retained 75% of the initial integrated PL intensity, which is 1.8 times higher than that of LSCs without carbon dots. The result underscores the possibility of enhancing LSC stability of by introducing a tandem structure [144].

Expected Applications of QD–LSC

One of the most prominent and widely studied applications of LSCs is BIPV, serving as a key component for achieving zero-energy buildings. LSCs are exceptionally well-suited for BIPV because they can cover not only opaque but also transparent parts of buildings (e.g., windows, spandrels, and curtain walls) with a variety of colors. Given that the estimated cost of triple-glazed ranges from 355 to 1035 €/m², the additional expense for luminophore and LSC installation, which is between 250 and 350 €/m², is considered affordable at present [52]. Further cost reduction are anticipated as the market for luminophore, particularly QDs, expands. If the lifetime of LSCs reach half that of PV, the extra energy generation by LSC will offset their additional cost [36]. Moreover, as illustrated in Fig. 6(a), LSCs can be adapted to fit curved surfaces, rendering them suitable for architectural envelope applications [150–152]. By employing small-sized block-shaped LSCs, a wide array of colors can be introduced to the building exterior, while LSCs manufactured with printed luminophores offer decorative options for buildings [68, 153, 154]. Beyond their esthetic enhancement, LSCs play a pivotal role in reducing the energy consumption of buildings by allowing daylight penetration and enhancing thermal insulation. Furthermore, studies propose integrating LSCs with chromatic glass to provide selective shading functionality [140]. Recent studies successfully have replaced toxic luminophores with eco-benign alternatives

and increased η_{opt}, as discussed in previous chapters. This progress address the remaining issues of luminophore toxicity and scalability of LSC. If further studies for easy installation methods for LSCs and their stability are conducted, they will successfully enter the market. The incorporation of BIPV featuring LSCs for energy generation within buildings will substantially contribute to the realization of zero-energy buildings.

Significant research efforts have been devoted to enhancing the $\eta_{LSC,PV}$ of LSCs for BIPV applications, focusing on improvements in luminophores and novel optical structures. Since 2020, studies investigating the actual energy generation potential of LSC in operational settings have been emerging. The research group of UbiQD Inc. analyzed the power generation capabilities of CuInS QD-based LSCs integrated into windows of a test model. As illustrated in Fig. 6(a) and (b), non-south-facing LSCs efficiently harness incident solar light, except for those facing north [146]. The study demonstrated the potential contribution of LSCs, regardless of the building's orientation, highlighting their ability to harness incident light from both the front and back sides simultaneously. Furthermore, theoretical analysis conducted based on the experiment suggested that installing LSCs with PVs on building rooftops leads to greater energy production compared to vertically oriented PVs, as depicted in Fig. 6(c) and (d) [147]. In two cities in the United States of America, Phoenix (33˚N, desert climate) and Albany (42 °N, temperate climate zone), both planar and wedge-shaped LSC configurations integrated with PVs are projected to generate more energy than PVs operating without LSCs. Moreover, incorporating LSCs into conventional PV systems will enhance their stability by minimizing current mismatching among cells caused by non-uniform light irradiation [155, 156]. The incident light will be redistributed through the wedge-shaped and planar LSCs, thereby mitigating local heating of PV cells due to current mismatches. This strategy contributes to improved power generation of the conventional PV system.

Another possible market for LSCs is noise barriers, which efficiently capture light incidents from both sides, as illustrated in Fig. 6(e–h). Given that LSCs comprise a glass substrate with a luminophore, they are effectively suited for noise mitigation. Figure 6(g) depicts a schematic of a vertically installed LSC for a noise barrier, wherein the LSC absorbs incident solar irradiation from both sides. Unlike conventional PV systems, which typically generate maximum power at noon, LSC noise barriers facing east or west maximize energy generation shortly after sunrise in the morning and just before sunset in the afternoon. The different energy generation behaviors of LSCs could compensate for the lower-energy production of conventional PVs during the early morning and sunset periods by reaching peak energy generation at those
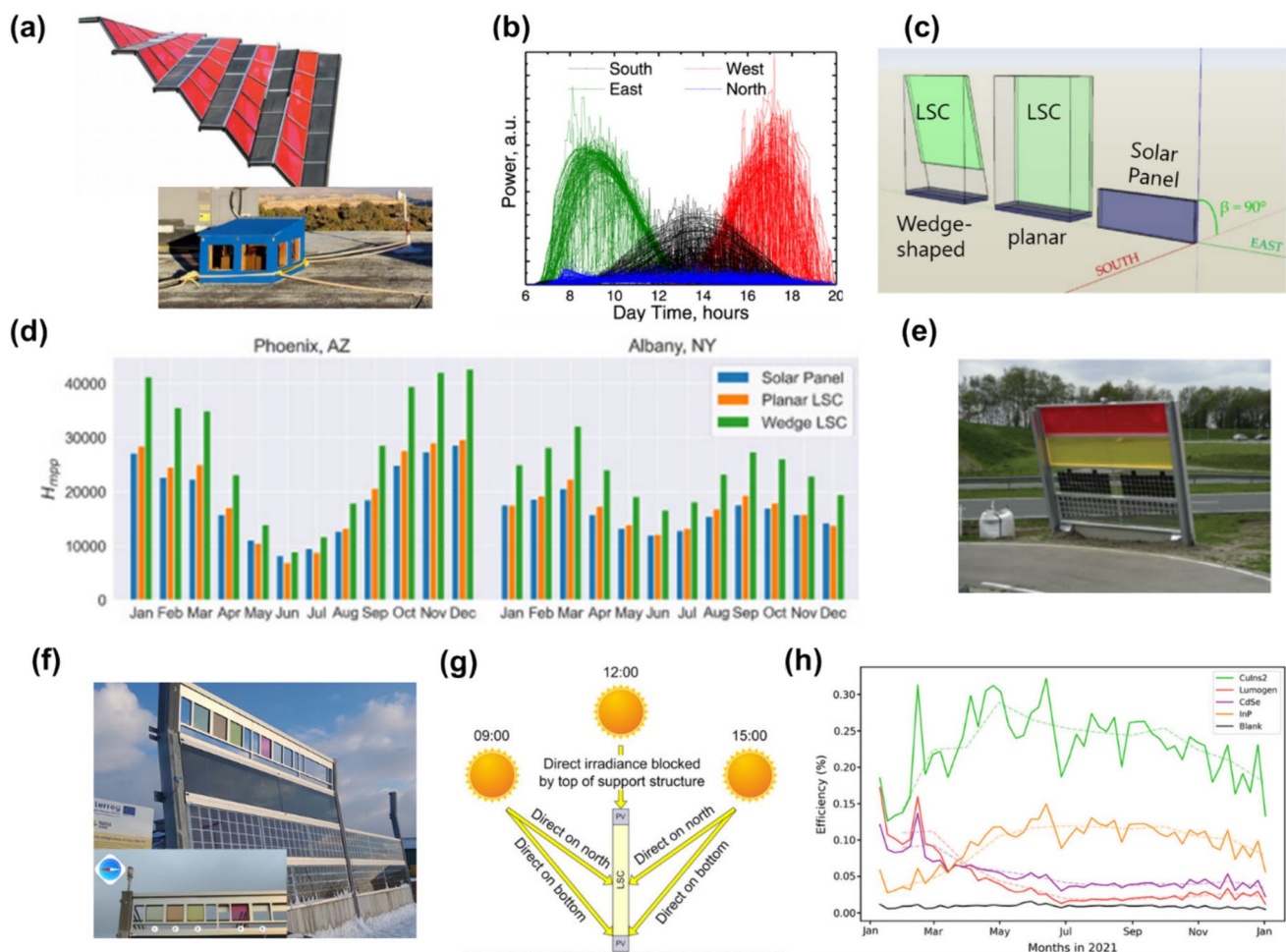
Fig. 6 **a** Canopy of a building consisting of PV modules (black) and LSC (red) (up) [145] and experimental model house with LSC-incorporated window (down) [146]. **b** Power generation of LSC-based window from the experimental model house facing different sides (Reprinted with permission [146], Copyright 2022, American Chemical Society.) Except for a north-facing LSC, the LSCs efficiently generate energy regardless of their direction. **c** Schematic of field-test LSCs: wedge-shaped LSC (left), planar LSC (middle), and a solar panel (right) facing south at a 90° tilt (Reprinted with permission

[147], Copyright 2017, Elsevier.) **d** Theoretically calculated annual energy generation of field-tested LSC installed at Phoenix, Arizona and Albany, New York (USA). **e, f** Photos of field-test LSC for noise barrier consisted of various luminophores (Reprinted with permission [148], Copyright 2022, Elsevier and [149] Copyright 2022, Wiley–VCH.) **g** Schematic of solar light irradiation to LSC during day time and **h** measured annual $\eta_{LSC,PV}$ of each LSC with different QDs

times. The energy generation data for various QD-based LSCs (CdSe/CdS/ZnS, CuInS$_2$/ZnS, and InP/ZnSe/ZnS) for 1 year (2021–2022) are shown in Fig. 6(h). Interestingly, the photo-brightening induced by incident light may alleviate the defects and trap states present in CuInS$_2$ and InP QDs, thereby leading to improved performance after long-term exposure to sunlight. This result suggests that LSCs incorporating CuInS$_2$ and InP QDs might generate more power in the field compared to lab-scale experiments due to the improved stability via photo-brightening effect.

In addition to traditional applications such as BIPV or noise barrier, the utilization of LSCs, leveraging their unique electro-optical properties, is diversifying into various new

fields. Emerging applications include optical communication, agriculture, and hydrogen generation. Integrated LSC systems hold promise as solutions for effective diagnosis of the human body and optical communication. The inherent advantage of employing LSCs lies in their ability to enhance the response of photodetectors and PVs by absorbing incident light through a large plate. Consequently, this would contribute to intensifying the signal while removing noise interference. Figure 7(a) depicts a schematic of an LSC designed for optical communication. In the absence of the optical fiber, the LSC can absorb light at specific wavelengths and concentrate it on the edge-mounted detector. Given the LSC's rapid response to incident light, combining
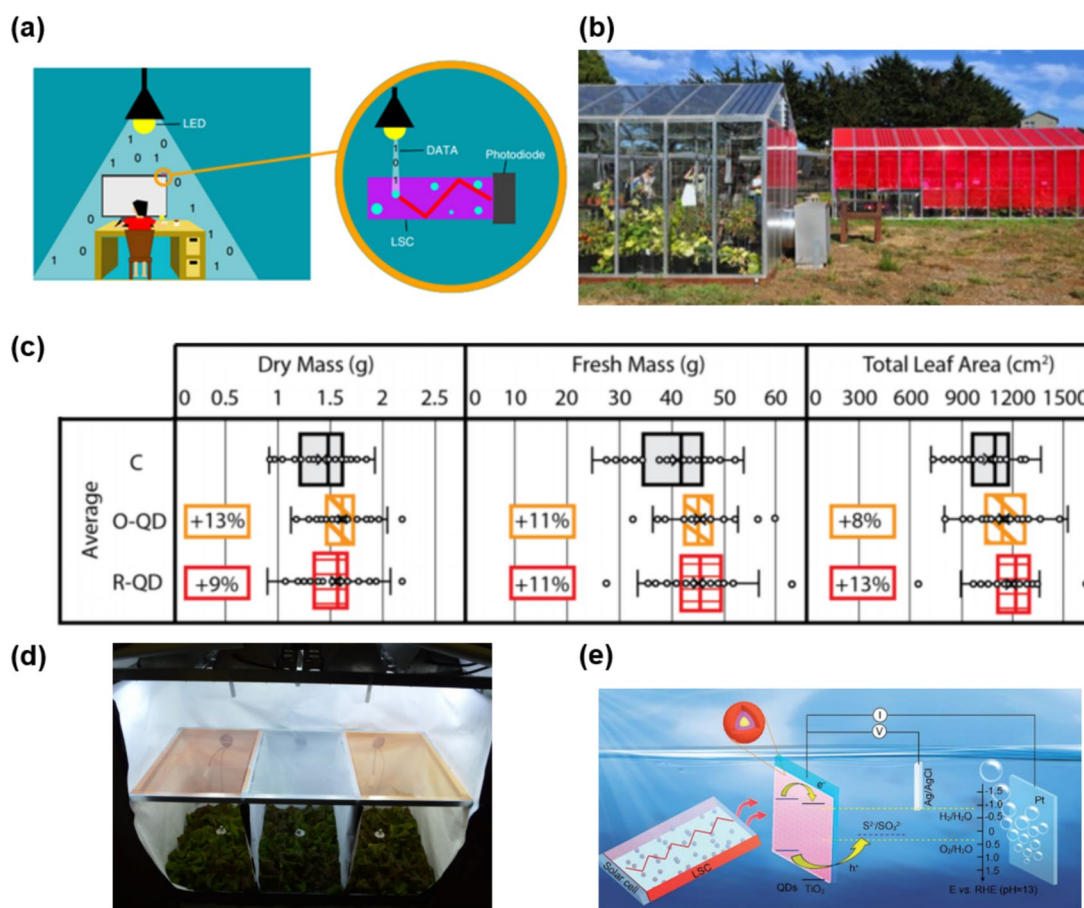
Fig. 7 **a** Schematic of optical communication with LSC. Without complicated optical fibers, it is possible to communicate the signal using LSC and impulse light sources. (Reprinted with permission [157], Copyright 2021, Springer Nature.) **b** Greenhouse with a PV cell-incorporated LSC (red) layer, whose energy generation is 37% higher than that of one without LSC (Reprinted with permission [39], Copyright 2016, AIP Publishing LLC). **c** Down-converting LSC layer for the cultivation of lettuce and **d** its experimental setup. The lettuce under orange (O-QD) and red (R-QD) grows larger and heavier than those under glass, (Reprinted with permission [158], Copyright 2021, American Chemical Society.) **e** Photoelectrochemical device for hydrogen production. The incorporation of LSC increases the stability of the system by down-converting high-energy photons (UV, deep blue light) to low-energy light (red light). (Reprinted with permission [159], Copyright 2019, The Royal Society of Chemistry.)

it with impulse lasers enables the feasibility of free-space optical communication systems operating at frequencies around MHz (~ 10^6 Hz). As a result, LSCs for optical communication can play a crucial role in transmitting light generated from LEDs without the need for a complicated optical fiber structure[157]. Recently, F. Meinardi et al. successfully demonstrated indoor visible light communication system using a conventional LED and CuInS$_2$ QD-based LSC. The LSC functioned as an optical antenna, receiving 32-bit data packets from LED and transmitting them to an edge-mounted photodetector. This work suggests that millimeter-scale optical communication is feasible using QD-based LSC and conventional LEDs [160]. Another possible application lies in the medical field. With the ability to be composed of flexible and biocompatible materials, LSCs could function as detectors for healthcare devices. For

example, they could be used as photodetectors for disease monitoring, heartbeat monitoring, virus detection, and other medical applications [161].

Another promising application of LSC involves harnessing energy at agriculture facilities. Traditionally, a crucial consideration in agriculture has been ensuring that crops receive sufficient sunlight during the daytime while maintaining optimal temperatures. Transparent greenhouses have facilitated consistent agricultural yields regardless of climatic conditions. Efforts to harness incoming solar radiation within greenhouses, their primary function, are actively underway, with significant advances being made toward achieving abundant energy generation by integrating LSCs into greenhouses. Figure 7(b) displays a photograph of two greenhouses, one with red-colored LSCs and the other with transparent glass. In this study, PVs were located

centrally between the glass and LSCs. Upon installing LSCs and transparent glass on the roofs of identical greenhouses, it was noted that PVs equipped with LSCs (22.9 W/m^2 at peak time) demonstrated superior efficiency (37% improvement) compared to PVs with transparent glass (16.8 W/m^2 at peak time) [39].

LSCs not only generate significant amounts of power but also contribute to ensuring high-quality crop yields by modifying the spectrum of incident solar light, as depicted in Fig. 7(c) and (d). The impact of LSCs on plant growth was assessed using lettuce covered with a polyethylene film doped with red and orange CuInS$_2$/ZnS QDs. The introduction of down-shifting LSCs resulted in the cultivation of lettuce with larger and fresher leaves, as demonstrated by their increased mass and size. The edible dry mass exhibited a respective increase of 13% and 9% under orange and red LSCs. Maximizing plant growth hinges on receiving ample light with the photosynthetically active radiation range, typically 400–700 nm for lettuce. Since the emission peaks of orange and red luminophores occur at 600 and 660 nm, respectively, re-emitted light falling within this range aids in accelerating lettuce growth [158]. Case studies conducted by a private company indicate that QD films designed for controlled light irradiance have improved the cultivation of tomatoes, cannabis, and geranium Furthermore, LSCs, by reshaping the solar spectrum, have been instrumental in promoting algae growth, thereby enhancing biomass energy productivity [162–164].

Reshaping incident light's spectrum via LSC may enhance the productivity of the clean-hydrogen fabrication process. Hydrogen stands as a promising energy storage system for sustainable energy development. Photoelectrochemical (PEC) water splitting, employing sunlight irradiation with electrical bias from PVs, represents one of the most efficient ways for hydrogen production. By leveraging photogenerated excitons and the electrical potential energy between two electrodes, PEC decomposes water into hydrogen and oxygen. To prevent photochemical degradation in the PEC system, it is imperative to down-convert high-energy photons from sunlight into lower-energy photons with a band gap well-suited to the photoanode of the PEC [165]. The spectrum of re-emitted light can be easily tuned in the QD-based LSCs, making them ideal for LSC integration into a PEC system to down-convert incident light for photoanode. Figure 7(e) illustrates the schematic of a water electrolysis device with an integrated LSC, wherein the photoanode is placed at the edge of the LSC. The photoanode of the PEC system is typically sensitive to high-energy photons, which may lead to photochemical degradation of the photoanode and the entire system. Hence, G. Liu et al. integrated a core/shell QD-based LSC into the photoanode of the PEC to modify incident light and attenuate high-energy photons.

The CdSe/CdS QD effectively absorbs UV and deep blue light and re-emits red light, energy levels similar to the bandgap of the photoanode. This coupling of LSC with PEC resulted in a marked enhancement in the photostability of the PEC system, leading to a 420% increase in hydrogen generation efficiency, which is higher than that of PEC without LSC [159]. Consequently, the attainable advantage of LSCs lies in their capacity to maximize the energy generation of other systems with which they are integrated.

Conclusion

The LSC represents a promising energy generation system comprising a waveguided plate with a luminophore. The maximum achievable concentration through the LSC is constrained by the re-absorption of emitted light and the escape of photons from the LSC. Consequently, most studies aimed at developing new luminophores and device structures to surpass these limits of LSC. The core/shell QDs have been intensively studied for luminophores of LSC due to their significant Stokes shift, near-unity η_{PLQY}, and controllable spectrum of re-emitted light. The engineering of QD, such as implementing giant shell structures, metal doping, and binary and ternary structures, has led to enhanced LSC performance. Moreover, optical engineering techniques, including selective reflectors, photonic crystals, and tandem structures, allow for the recycling of escaping photons. As a result, many LSCs for BIPV applications are currently undergoing field tests to validate their performance under real operating conditions. Furthermore, the application of LSC is now expanding in various new fields, such as optical communication, agriculture, and other energy generation systems. Once the remarkable advantages of QD-based LSCs are harnessed through device engineering and the development of new materials, LSCs are poised to capture a considerable portion of the future energy market.

Declarations

Conflict of Interest The authors declare no competing financial interest.

References

1. C. Ippen, T. Greco, Y. Kim, J. Kim, M.S. Oh, C.J. Han, A. Wedel, Znse/zns quantum dots as emitting material in blue qd-leds with narrow emission peak and wavelength tunability. Org. Electron. **15**, 126 (2014)

2. P. Yang, M. Ando, T. Taguchi, N. Murase, Highly luminescent cdse/cd x zn1–x s quantum dots with narrow spectrum and widely tunable wavelength. J. Phys. Chem. C **115**, 14455 (2011)

3. T. Kim, D. Shin, M. Kim, H. Kim, E. Cho, M. Choi, J. Kim, E. Jang, S. Jeong, Development of group iii–v colloidal quantum dots for optoelectronic applications. ACS Energy Lett. **8**, 447 (2022)

4. J. Kim, J. Roh, M. Park, C. Lee, Recent advances and challenges of colloidal quantum dot light-emitting diodes for display applications. Adv. Mater. **36**(20), 2212220 (2023)

5. D.A. Taylor, J.A. Teku, S. Cho, W.-S. Chae, S.-J. Jeong, J.-S. Lee, Importance of surface functionalization and purification for narrow fwhm and bright green-emitting inp core–multishell quantum dots via a two-step growth process. Chem. Mater. **33**, 4399 (2021)

6. G.D. Cha, D.-H. Kim, D.C. Kim, Wearable and implantable light-emitting diodes and their biomedical applications. Korean J. Chem. Eng. **41**(1), 1–24 (2024)

7. W.K. Bae, J. Lim, Nanostructured colloidal quantum dots for efficient electroluminescence devices. Korean J. Chem. Eng. **36**, 173 (2019)

8. T.W. Nam, M.-J. Choi, Y.S. Jung, Ultrahigh-resolution quantum dot patterning for advanced optoelectronic devices. Chem. Commun. **59**, 2697 (2023)

9. B. Li, M. Lu, J. Feng, J. Zhang, P.M. Smowton, J.I. Sohn, I.-K. Park, H. Zhong, B. Hou, Colloidal quantum dot hybrids: an emerging class of materials for ambient lighting. J. Mater. Chem. C **8**, 10676 (2020)

10. S. Park, M.K. Son, S.K. Kim, M.S. Jeong, K. Prabakar, H.J. Kim, The effects of electrolyte additives on the cell performances of cds/cdse quantum dot sensitized solar cells. Korean J. Chem. Eng. **30**, 2088 (2013)

11. H.J. Yun, J. Lim, J. Roh, D.C.J. Neo, M. Law, V.I. Klimov, Solution-processable integrated cmos circuits based on colloidal cuinse2 quantum dots. Nat. Commun. **11**, 5280 (2020)

12. E. Hwang, B. Lee, Synthesis of a fluorescence sensor based on carbon quantum dots for detection of bisphenol a in aqueous solution. Korean J. Chem. Eng. **39**, 1324 (2022)

13. G. Whitworth, M. Dalmases, N. Taghipour, G. Konstantatos, Solution-processed pbs quantum dot infrared laser with room-temperature tunable emission in the optical telecommunications window. Nat. Photonics **15**, 738 (2021)

14. Y.-S. Park, J. Roh, B.T. Diroll, R.D. Schaller, V.I. Klimov, Colloidal quantum dot lasers. Nat. Rev. Mater. **6**, 382 (2021)

15. Z. Cui, D. Yang, S. Qin, Z. Wen, H. He, S. Mei, W. Zhang, G. Xing, C. Liang, R. Guo, Advances, challenges, and perspectives for heavy-metal-free blue-emitting indium phosphide quantum dot light-emitting diodes. Adv. Opt. Mater. **11**, 2202036 (2023)

16. D. Tian, H. Ma, G. Huang, M. Gao, F. Cai, Y. Fang, C. Li, X. Jiang, A. Wang, S. Wang, A review on quantum dot light-emitting diodes: from materials to applications. Adv. Opt. Mater. **11**, 2201965 (2023)

17. H.J. Jang, J.Y. Lee, G.W. Baek, J. Kwak, J.-H. Park, Progress in the development of the display performance of ar, vr, qled and oled devices in recent years. J. Inform. Disp. **23**, 1 (2022)

18. H. Lee, H.-J. Song, M. Shim, C. Lee, Towards the commercialization of colloidal quantum dot solar cells: perspectives on device structures and manufacturing. Energy Environ. Sci. **13**, 404 (2020)

19. Y. Pu, F. Cai, D. Wang, J.-X. Wang, J.-F. Chen, Colloidal synthesis of semiconductor quantum dots toward large-scale production: a review. Ind. Eng. Chem. Res. **57**, 1790 (2018)

20. Y.-F. Ma, Y.-M. Wang, J. Wen, A. Li, X.-L. Li, M. Leng, Y.-B. Zhao, Z.-H. Lu, Review of roll-to-roll fabrication techniques for colloidal quantum dot solar cells. J. Electron. Sci. Technol. **21**, 100189 (2023)

21. B.W. Jo, A. Lee, K.H. Ahn, S.J. Lee, Evaluation of jet performance in drop-on-demand (dod) inkjet printing. Korean J. Chem. Eng. **26**, 339 (2009)

22. C. Wei, W. Su, J. Li, B. Xu, Q. Shan, Y. Wu, F. Zhang, M. Luo, H. Xiang, Z. Cui, A universal ternary-solvent-ink strategy toward efficient inkjet-printed perovskite quantum dot light-emitting diodes. Adv. Mater. **34**, 2107798 (2022)

23. B.G. Jeong, D. Hahm, J.W. Park, J.Y. Kim, H.-E. Song, M.G. Kang, S. Jeong, G. Kang, W.K. Bae, H.-J. Song, Colorful opaque photovoltaic modules with down-converting inp/znsexs1-x quantum dot layers. Nano Energy **77**, 105169 (2020)

24. Z. Hu, Y. Yin, M.U. Ali, W. Peng, S. Zhang, D. Li, T. Zou, Y. Li, S. Jiao, S.-J. Chen, Inkjet printed uniform quantum dots as color conversion layers for full-color oled displays. Nanoscale **12**, 2103 (2020)

25. S. Mallick, A. Pal, A. Kumar, M.P. Sk, *Quantum dots as photon down-conversion materials* (Advances in electronic materials for clean energy conversion and storage applications, Elsevier, 2023), pp.247–264

26. S. Sadeghi, H. Bahmani Jalali, R. Melikov, B. Ganesh Kumar, M. Mohammadi Aria, C.W. Ow-Yang, S. Nizamoglu, Stokes-shift-engineered indium phosphide quantum dots for efficient luminescent solar concentrators. ACS Appl. Mater. Interfaces **10**, 12975 (2018)

27. X. Tong, X.T. Kong, C. Wang, Y. Zhou, F. Navarro-Pardo, D. Barba, D. Ma, S. Sun, A.O. Govorov, H. Zhao, Optoelectronic properties in near-infrared colloidal heterostructured pyramidal "giant" core/shell quantum dots. Adv. Sci. **5**, 1800656 (2018)

28. B.G. Jeong, Y.-S. Park, J.H. Chang, I. Cho, J.K. Kim, H. Kim, K. Char, J. Cho, V.I. Klimov, P. Park, Colloidal spherical quantum wells with near-unity photoluminescence quantum yield and suppressed blinking. ACS Nano **10**, 9297 (2016)

29. H. Lee, H.J. Song, Current status and perspective of colored photovoltaic modules. Wiley Interdiscipl. Rev.: Energy Environ. **10**, e403 (2021)

30. T.H. Le, D.H. Lee, J.H. Kim, S.J. Park, Synthesis of enhanced fluorescent graphene quantum dots for catecholamine neurotransmitter sensing. Korean J. Chem. Eng. **37**, 1000 (2020)

31. J. Bomm, A. Büchtemann, A.J. Chatten, R. Bose, D.J. Farrell, N.L. Chan, Y. Xiao, L.H. Slooff, T. Meyer, A. Meyer, Fabrication and full characterization of state-of-the-art quantum dot luminescent solar concentrators. Sol. Energy Mater. Sol. Cells **95**, 2087 (2011)

32. Y. Zhou, H. Zhao, D. Ma, F. Rosei, Harnessing the properties of colloidal quantum dots in luminescent solar concentrators. Chem. Soc. Rev. **47**, 5866 (2018)

33. F. Meinardi, H. McDaniel, F. Carulli, A. Colombo, K.A. Velizhanin, N.S. Makarov, R. Simonutti, V.I. Klimov, S. Brovelli, Highly efficient large-area colourless luminescent solar concentrators using heavy-metal-free colloidal quantum dots. Nat. Nanotechnol. **10**, 878 (2015)

34. J.A. Sol, G.H. Timmermans, A.J. van Breugel, A.P. Schenning, M.G. Debije, Multistate luminescent solar concentrator "smart" windows. Adv. Energy Mater. **8**, 1702922 (2018)

35. A. Jiménez-Solano, J.M. Delgado-Sánchez, M.E. Calvo, J.M. Miranda-Muñoz, G. Lozano, D. Sancho, E. Sánchez-Cortezón, H. Míguez, Design and realization of transparent solar modules based on luminescent solar concentrators integrating

nanostructured photonic crystals. Prog. Photovolt. Res. Appl. **23**, 1785 (2015)

36. T.K. Baikie, B. Daiber, E. Kensington, J. Xiao, N.C. Greenham, B. Ehrler, A. Rao, Revealing the potential of luminescent solar concentrators in real-world environments. Joule **8**(3), 799–816 (2024)

37. X. Li, J. Qi, J. Zhu, Y. Jia, Y. Liu, Y. Li, H. Liu, G. Li, K. Wu, Low-loss, high-transparency luminescent solar concentrators with a bioinspired self-cleaning surface. J. Phys. Chem. Lett. **13**, 9177 (2022)

38. M.R. Bergren, N.S. Makarov, K. Ramasamy, A. Jackson, R. Guglielmetti, H. McDaniel, High-performance cuins2 quantum dot laminated glass luminescent solar concentrators for windows. ACS Energy Lett. **3**, 520 (2018)

39. C. Corrado, S.W. Leow, M. Osborn, I. Carbone, K. Hellier, M. Short, G. Alers, S.A. Carter, Power generation study of luminescent solar concentrator greenhouse. J. Renew. Sustain Energy **8**, 043502 (2016)

40. R. Reisfeld, S. Neuman, Planar solar energy converter and concentrator based on uranyl-doped glass. Nature **274**, 144–155 (1978)

41. R. Reisfeld, Y. Kalisky, Improved planar solar converter based on uranyl neodymium and holmium glasses. Nature **283**, 281 (1980)

42. W.H. Weber, J. Lambe, Luminescent greenhouse collector for solar radiation. Appl. Opt. **15**, 2299 (1976)

43. A. Goetzberger, W. Greube, Solar energy conversion with fluorescent collectors. Appl. Phys. **14**, 123 (1977)

44. A. S.Glassner. An introduction to ray tracing, Morgan Kaufmann (1989)

45. Z. Xu, M. Portnoi, I. Papakonstantinou, Micro-cone arrays enhance outcoupling efficiency in horticulture luminescent solar concentrators. Opt. Lett. **48**, 183 (2023)

46. S. Woei Leow, C. Corrado, M. Osborn, M. Isaacson, G. Alers, S.A. Carter, Analyzing luminescent solar concentrators with front-facing photovoltaic cells using weighted monte carlo ray tracing. J. Appl. Phys. (2013). https://doi.org/10.1063/1.4807413

47. C. Corrado, S.W. Leow, M. Osborn, E. Chan, B. Balaban, S.A. Carter, Optimization of gain and energy conversion efficiency using front-facing photovoltaic cell luminescent solar concentrordesign. Sol. Energy Mater. Sol. Cells **111**, 74 (2013)

48. H.-J. Song, B.G. Jeong, J. Lim, D.C. Lee, W.K. Bae, V.I. Klimov, Performance limits of luminescent solar concentrators tested with seed/quantum-well quantum dots in a selective-reflector-based optical cavity. Nano Lett. **18**, 395 (2018)

49. K. Gungor, J. Du, V.I. Klimov, General trends in the performance of quantum dot luminescent solar concentrators (lscs) revealed using the "effective lsc quality factor." ACS Energy Lett. **7**, 1741 (2022)

50. V.I. Klimov, T.A. Baker, J. Lim, K.A. Velizhanin, H. McDaniel, Quality factor of luminescent solar concentrators and practical concentration limits attainable with semiconductor quantum dots. ACS Photonics **3**, 1138 (2016)

51. S. Castelletto, A. Boretti, Luminescence solar concentrators: a technology update. Nano Energy **109**, 108269 (2023)

52. B.S. Richards, I.A. Howard, Luminescent solar concentrators for building integrated photovoltaics: opportunities and challenges. Energy Environ. Sci. **16**, 3214 (2023)

53. L.R. Wilson, E. Klampaftis, B.S. Richards, Enhancement of power output from a large-area luminescent solar concentrator with 48× concentration via solar cell current matching. IEEE J. Photovolt. **7**, 802 (2017)

54. A. Anand, M.L. Zaffalon, G. Gariano, A. Camellini, M. Gandini, R. Brescia, C. Capitani, F. Bruni, V. Pinchetti, M. Zavelani-Rossi, F. Meinardi, S.A. Crooker, S. Brovelli, Evidence for the band-edge exciton of cuins2 nanocrystals enables record efficient large-area luminescent solar concentrators. Adv. Func. Mater. **30**, 1906629 (2020)

55. N. Aste, L.C. Tagliabue, C. Del Pero, D. Testa, R. Fusco, Performance analysis of a large-area luminescent solar concentrator module. Renew. Energy **76**, 330 (2015)

56. J. Zhang, M. Wang, Y. Zhang, H. He, W. Xie, M. Yang, J. Ding, J. Bao, S. Sun, C. Gao, Optimization of large-size glass laminated luminescent solar concentrators. Sol. Energy **117**, 260 (2015)

57. G. Gu, Z. Zheng, H. Zhang, Y. Zhang, Z. Gan, R. Huang, X. Zhang, Re-absorption-free perovskite quantum dots for boosting the efficiency of luminescent solar concentrator. J. Lumin. **248**, 118963 (2022)

58. P. Xia, H. Sun, H. Guo, K. Zhao, C. Liang, C. Lu, Z. Wang, S. Xu, C. Wang, Luminescent solar concentrator with advanced structure for reabsorption loss suppression and synergistic energy harvesting. Adv. Funct. Mater. (2024). https://doi.org/10.1002/adfm.202401121

59. H.J. Lee, S. Im, D. Jung, K. Kim, J.A. Chae, J. Lim, J.W. Park, D. Shin, K. Char, B.G. Jeong, Coherent heteroepitaxial growth of i-iii-vi2 ag (in, ga) s2 colloidal nanocrystals with near-unity quantum yield for use in luminescent solar concentrators. Nat. Commun. **14**, 3779 (2023)

60. C. Papucci, T.A. Geervliet, D. Franchi, O. Bettucci, A. Mordini, G. Reginato, F. Picchioni, A. Pucci, M. Calamante, L. Zani, Green/yellow-emitting conjugated heterocyclic fluorophores for luminescent solar concentrators. Eur. J. Org. Chem. **2018**, 2657 (2018)

61. I. Coropceanu, M.G. Bawendi, Core/shell quantum dot based luminescent solar concentrators with reduced reabsorption and enhanced efficiency. Nano Lett. **14**, 4097 (2014)

62. C.S. Erickson, L.R. Bradshaw, S. McDowall, J.D. Gilbertson, D.R. Gamelin, D.L. Patrick, Zero-reabsorption doped-nanocrystal luminescent solar concentrators. ACS Nano **8**, 3461 (2014)

63. Q. Jing, X. Meng, C. Wang, H. Zhao, Exciton dynamic in pyramidal inp/znse quantum dots for luminescent solar concentrators. ACS Appl. Nano Mater. **6**, 4449 (2023)

64. Y. Zhou, D. Benetti, X. Tong, L. Jin, Z.M. Wang, D. Ma, H. Zhao, F. Rosei, Colloidal carbon dots based highly stable luminescent solar concentrators. Nano Energy **44**, 378 (2018)

65. T. de Bruin, W. van Sark, Investigation of quantum dot luminescent solar concentrator single, double and triple structures: a ray tracing simulation study. Ceram. Int. **49**, 24454 (2023)

66. I.A. Carbone, K.R. Frawley, M.K. McCann, Flexible, front-facing luminescent solar concentrators fabricated from lumogen f red 305 and polydimethylsiloxane. Int. J. Photoenergy **2019**, 1–9 (2019)

67. Z. Krumer, W.G. van Sark, R.E. Schropp, C. de Mello Donegá, Compensation of self-absorption losses in luminescent solar concentrators by increasing luminophore concentration. Sol. Energy Mater. Sol. Cells **167**, 133 (2017)

68. A. Reinders, R. Kishore, L. Slooff, W. Eggink, Luminescent solar concentrator photovoltaic designs. Jpn. J. Appl. Phys. **57**, 08RD10 (2018)

69. L.H. Slooff, E.E. Bende, A.R. Burgers, T. Budel, M. Pravettoni, R.P. Kenny, E.D. Dunlop, A. Büchtemann, A luminescent solar concentrator with 7.1% power conversion efficiency. Phys. Status Solidi RRL Rapid Res. Lett. **2**, 257 (2008)

70. F. Corsini, A. Nitti, E. Tatsi, G. Mattioli, C. Botta, D. Pasini, G. Griffini, Large-area semi-transparent luminescent solar concentrators based on large stokes shift aggregation-induced fluorinated emitters obtained through a sustainable synthetic approach. Adv. Opt. Mater. **9**, 2100182 (2021)

71. C. Ceriani, F. Corsini, G. Mattioli, S. Mattiello, D. Testa, R. Po, C. Botta, G. Griffini, L. Beverina, Sustainable by design, large stokes shift benzothiadiazole derivatives for efficient luminescent solar concentrators. J. Mater. Chem. C **9**, 14815 (2021)

72. S. Mattiello, A. Sanzone, F. Bruni, M. Gandini, V. Pinchetti, A. Monguzzi, I. Facchinetti, R. Ruffo, F. Meinardi, G. Mattioli, Chemically sustainable large stokes shift derivatives for high-performance large-area transparent luminescent solar concentrators. Joule **4**, 1988 (2020)

73. R. Inman, G. Shcherbatyuk, D. Medvedko, A. Gopinathan, S. Ghosh, Cylindrical luminescent solar concentrators with near-infrared quantum dots. Opt. Express **19**, 24308 (2011)

74. F. Meinardi, A. Colombo, K.A. Velizhanin, R. Simonutti, M. Lorenzon, L. Beverina, R. Viswanatha, V.I. Klimov, S. Brovelli, Large-area luminescent solar concentrators based on 'stokes-shift-engineered' nanocrystals in a mass-polymerized pmma matrix. Nat. Photonics **8**, 392 (2014)

75. G. Shcherbatyuk, R. Inman, C. Wang, R. Winston, S. Ghosh, Viability of using near infrared pbs quantum dots as active materials in luminescent solar concentrators. Appl. Phys. Lett. (2010). https://doi.org/10.1063/1.3422485

76. R. Koole, P. Liljeroth, C. de Mello Donegá, D. Vanmaekelbergh, A. Meijerink, Electronic coupling and exciton energy transfer in cdte quantum-dot molecules. J. Am. Chem. Soc. **128**, 10436 (2006)

77. C. Woelfle, R.O. Claus, Transparent and flexible quantum dot–polymer composites using an ionic liquid as compatible polymerization medium. Nanotechnology **18**, 025402 (2006)

78. P. Wu, X.-P. Yan, Doped quantum dots for chemo/biosensing and bioimaging. Chem. Soc. Rev. **42**, 5489 (2013)

79. M. Liu, W. Yao, C. Li, Z. Wu, L. Li, Tuning emission and stokes shift of cds quantum dots via copper and indium co-doping. RSC Adv. **5**, 628 (2015)

80. D. Mocatta, G. Cohen, J. Schattner, O. Millo, E. Rabani, U. Banin, Heavily doped semiconductor nanocrystal quantum dots. Science **332**, 77 (2011)

81. S. Roy, C. Tuinenga, F. Fungura, P. Dagtepe, V. Chikan, J. Jasinski, Progress toward producing n-type cdse quantum dots: tin and indium doped cdse quantum dots. J. Phys. Chem. C **113**, 13008 (2009)

82. V.K. Sharma, B. Guzelturk, T. Erdem, Y. Kelestemur, H.V. Demir, Tunable white-light-emitting mn-doped znse nanocrystals. ACS Appl. Mater. Interfaces **6**, 3654 (2014)

83. R. Beaulac, P.I. Archer, S.T. Ochsenbein, D.R. Gamelin, Mn2+-doped cdse quantum dots: New inorganic materials for spin-electronics and spin-photonics. Adv. Func. Mater. **18**, 3873 (2008)

84. S. Gul, J.K. Cooper, P.-A. Glans, J. Guo, V.K. Yachandra, J. Yano, J.Z. Zhang, Effect of al3+ co-doping on the dopant local structure, optical properties, and exciton dynamics in cu+-doped znse nanocrystals. ACS Nano **7**, 8680 (2013)

85. M. Sharma, K. Gungor, A. Yeltik, M. Olutas, B. Guzelturk, Y. Kelestemur, T. Erdem, S. Delikanli, J.R. McBride, H.V. Demir, Near-unity emitting copper-doped colloidal semiconductor quantum wells for luminescent solar concentrators. Adv. Mater. **29**, 1700821 (2017)

86. P. Modlitbová, P. Pořízka, K. Novotný, J. Drbohlavová, I. Chamradová, Z. Farka, H. Zlámalová-Gargošová, T. Romih, J. Kaiser, Short-term assessment of cadmium toxicity and uptake from different types of cd-based quantum dots in the model plant allium cepa l. Ecotoxicol. Environ. Saf. **153**, 23 (2018)

87. G. Hong, J.T. Robinson, Y. Zhang, S. Diao, A.L. Antaris, Q. Wang, H. Dai, In vivo fluorescence imaging with ag2s quantum dots in the second near-infrared region. Angew. Chem. Int. Ed. **51**, 9818 (2012)

88. Y.-P. Gu, R. Cui, Z.-L. Zhang, Z.-X. Xie, D.-W. Pang, Ultrasmall near-infrared ag2se quantum dots with tunable fluorescence for in vivo imaging. J. Am. Chem. Soc. **134**, 79 (2012)

89. G.R. Chaudhary, P. Bansal, S. Mehta, Recyclable cus quantum dots as heterogeneous catalyst for biginelli reaction under solvent free conditions. Chem. Eng. J. **243**, 217 (2014)

90. K. Kaviyarasu, A. Ayeshamariam, E. Manikandan, J. Kennedy, R. Ladchumananandasivam, U.U. Gomes, M. Jayachandran, M. Maaza, Solution processing of cuse quantum dots: Photocatalytic activity under rhb for uv and visible-light solar irradiation. Mater. Sci. Eng. B **210**, 1 (2016)

91. S. Sadeghi, H.B. Jalali, S.B. Srivastava, R. Melikov, I. Baylam, A. Sennaroglu, S. Nizamoglu, High-performance, large-area, and ecofriendly luminescent solar concentrators using copper-doped inp quantum dots. iScience **23**, 101272 (2020)

92. Y.-H. Won, O. Cho, T. Kim, D.-Y. Chung, T. Kim, H. Chung, H. Jang, J. Lee, D. Kim, E. Jang, Highly efficient and stable inp/znse/zns quantum dot light-emitting diodes. Nature **575**, 634 (2019)

93. Y. Li, X. Hou, X. Dai, Z. Yao, L. Lv, Y. Jin, X. Peng, Stoichiometry-controlled inp-based quantum dots: Synthesis, photoluminescence, and electroluminescence. J. Am. Chem. Soc. **141**, 6448 (2019)

94. D. Hahm, J.H. Chang, B.G. Jeong, P. Park, J. Kim, S. Lee, J. Choi, W.D. Kim, S. Rhee, J. Lim, Design principle for bright, robust, and color-pure inp/znse x s1–x/zns heterostructures. Chem. Mater. **31**, 3476 (2019)

95. Z. Song, Z. Zheng, Y. Zhang, X. Cao, S. Li, H. Zhang, C. Luo, Y. Li, X. Zhang, The trade-off between optical efficiency and aesthetic properties of inp/zns quantum dots based luminescent solar concentrators. J. Lumin. **256**, 119622 (2023)

96. C.K. Gordon, R.F. Hogg, M.W. Brett, L.D. Browne, D.M. de Clercq, M.B. Price, N.J. Davis, Performance evaluation of solid state luminescent solar concentrators based on inp/zns-rhodamine 101 hybrid inorganic–organic luminophores. J. Phys. Chem. C **126**, 19803 (2022)

97. W. Zhang, S. Ding, W. Zhuang, D. Wu, P. Liu, X. Qu, H. Liu, H. Yang, Z. Wu, K. Wang, Inp/zns/zns core/shell blue quantum dots for efficient light-emitting diodes. Adv. Func. Mater. **30**, 2005303 (2020)

98. J. Lee, H. Jo, M. Choi, S. Park, J. Oh, K. Lee, Y. Bae, S. Rhee, J. Roh, Recent progress on quantum dot patterning technologies for commercialization of qd-leds: Current status, future prospects, and exploratory approaches. Small Methods **n/a**, 2301224 (2024)

99. E. Jang, H. Jang, Review: quantum dot light-emitting diodes. Chem. Rev. **123**, 4663 (2023)

100. A. Fuhr, H.J. Yun, S.A. Crooker, V.I. Klimov, Spectroscopic and magneto-optical signatures of cu1+ and cu2+ defects in copper indium sulfide quantum dots. ACS Nano **14**, 2212 (2020)

101. Y. You, X. Tong, W. Wang, J. Sun, P. Yu, H. Ji, X. Niu, Z.M. Wang, Eco-friendly colloidal quantum dot-based luminescent solar concentrators. Adv. Sci. **6**, 1801967 (2019)

102. D. Pan, L. An, Z. Sun, W. Hou, Y. Yang, Z. Yang, Y. Lu, Synthesis of cu− in− s ternary nanocrystals with tunable structure and composition. J. Am. Chem. Soc. **130**, 5620 (2008)

103. C. Li, W. Chen, D. Wu, D. Quan, Z. Zhou, J. Hao, J. Qin, Y. Li, Z. He, K. Wang, Large stokes shift and high efficiency luminescent solar concentrator incorporated with cuins2/zns quantum dots. Sci. Rep. **5**, 17777 (2015)

104. A.R.M. Velarde, E.R. Bartlett, N.S. Makarov, C. Castañeda, A. Jackson, K. Ramasamy, M.R. Bergren, H. McDaniel, Optimizing the aesthetics of high-performance cuins2/zns quantum dot luminescent solar concentrator windows. ACS Appl. Energy Mater. **3**, 8159 (2020)

105. W. Hoisang, T. Uematsu, T. Torimoto, S. Kuwabata, Surface ligand chemistry on quaternary ag (in x ga 1–x) s 2 semiconductor quantum dots for improving photoluminescence properties. Nanoscale Adv. **4**, 849 (2022)

106. T. Kameyama, M. Kishi, C. Miyamae, D.K. Sharma, S. Hirata, T. Yamamoto, T. Uematsu, M. Vacha, S. Kuwabata, T. Torimoto, Wavelength-tunable band-edge photoluminescence of

nonstoichiometric ag–in–s nanoparticles via ga3+ doping. ACS Appl. Mater. Interfaces **10**, 42844 (2018)

107. H.J. Lee, S. Im, D. Jung, K. Kim, J.A. Chae, J. Lim, J.W. Park, D. Shin, K. Char, B.G. Jeong, J.-S. Park, E. Hwang, D.C. Lee, Y.-S. Park, H.-J. Song, J.H. Chang, W.K. Bae, Coherent heteroepitaxial growth of i-iii-vi2 ag(in, ga)s2 colloidal nanocrystals with near-unity quantum yield for use in luminescent solar concentrators. Nat. Commun. **14**, 3779 (2023)

108. H.S. Heo, J.H. Jo, S.J. Lee, C. Yun, S.-H. Choi, J.H. Lee, K. Lee, Fabrication of cross-linked quantum dot/colorless-polyimide nanocomposites for highly efficient and long-term stable light-emitting diodes. Chem. Mater. **34**, 6958 (2022)

109. H. Li, K. Wu, J. Lim, H.-J. Song, V.I. Klimov, Doctor-blade deposition of quantum dots onto standard window glass for low-loss large-area luminescent solar concentrators. Nat. Energy **1**, 16157 (2016)

110. J. Li, H. Zhao, X. Zhao, X. Gong, Red and yellow emissive carbon dots integrated tandem luminescent solar concentrators with significantly improved efficiency. Nanoscale **13**, 9561 (2021)

111. H. Zhao, G. Liu, G. Han, High-performance laminated luminescent solar concentrators based on colloidal carbon quantum dots. Nanoscale Adv. **1**, 4888 (2019)

112. H. Zhao, D. Benetti, X. Tong, H. Zhang, Y. Zhou, G. Liu, D. Ma, S. Sun, Z.M. Wang, Y. Wang, Efficient and stable tandem luminescent solar concentrators based on carbon dots and perovskite quantum dots. Nano Energy **50**, 756 (2018)

113. H. Zhao, R. Sun, Z. Wang, K. Fu, X. Hu, Y. Zhang, Zero-dimensional perovskite nanocrystals for efficient luminescent solar concentrators. Adv. Func. Mater. **29**, 1902262 (2019)

114. H. Zhao, Y. Zhou, D. Benetti, D. Ma, F. Rosei, Perovskite quantum dots integrated in large-area luminescent solar concentrators. Nano Energy **37**, 214 (2017)

115. F. Meinardi, S. Ehrenberg, L. Dhamo, F. Carulli, M. Mauri, F. Bruni, R. Simonutti, U. Kortshagen, S. Brovelli, Highly efficient luminescent solar concentrators based on earth-abundant indirect-bandgap silicon quantum dots. Nat. Photonics **11**, 177 (2017)

116. S.K. Hill, R. Connell, C. Peterson, J. Hollinger, M.A. Hillmyer, U. Kortshagen, V.E. Ferry, Silicon quantum dot–poly (methyl methacrylate) nanocomposites with reduced light scattering for luminescent solar concentrators. ACS Photonics **6**, 170 (2018)

117. Y. Li, P. Miao, W. Zhou, X. Gong, X. Zhao, N-doped carbon-dots for luminescent solar concentrators. J. Mater. Chem. A **5**, 21452 (2017)

118. H. Zhao, G. Liu, S. You, F.V. Camargo, M. Zavelani-Rossi, X. Wang, C. Sun, B. Liu, Y. Zhang, G. Han, Gram-scale synthesis of carbon quantum dots with a large stokes shift for the fabrication of eco-friendly and high-efficiency luminescent solar concentrators. Energy Environ. Sci. **14**, 396 (2021)

119. X. Luo, T. Ding, X. Liu, Y. Liu, K. Wu, Quantum-cutting luminescent solar concentrators using ytterbium-doped perovskite nanocrystals. Nano Lett. **19**, 338 (2018)

120. T.A. Cohen, T.J. Milstein, D.M. Kroupa, J.D. MacKenzie, C.K. Luscombe, D.R. Gamelin, Quantum-cutting yb 3+-doped perovskite nanocrystals for monolithic bilayer luminescent solar concentrators. J. Mater. Chem. A **7**, 9279 (2019)

121. M. Wei, F.P.G. de Arquer, G. Walters, Z. Yang, L.N. Quan, Y. Kim, R. Sabatini, R. Quintero-Bermudez, L. Gao, J.Z. Fan, F. Fan, A. Gold-Parker, M.F. Toney, E.H. Sargent, Ultrafast narrowband exciton routing within layered perovskite nanoplatelets enables low-loss luminescent solar concentrators. Nat. Energy **4**, 197 (2019)

122. Y. Bai, M. Hao, S. Ding, P.F. Chen, L. Wang, Surface chemistry engineering of perovskite quantum dots: Strategies, applications, and perspectives. Adv. Mater. **34**, 2105958 (2022)

123. J. Tong, J. Luo, L. Shi, J. Wu, L. Xu, J. Song, P. Wang, H. Li, Z. Deng, Fabrication of highly emissive and highly stable perovskite nanocrystal-polymer slabs for luminescent solar concentrators. J. Mater. Chem. A **7**, 4872 (2019)

124. J. Kim, H.-J. Song, Strategies for efficient and stable colored perovskite module with bragg reflector and luminescent down-shifting layer. Cell Rep. Phys. Sci. **5**, 102070 (2024)

125. J. Wei, Q. Wang, J. Huo, F. Gao, Z. Gan, Q. Zhao, H. Li, Mechanisms and suppression of photoinduced degradation in perovskite solar cells. Adv. Energy Mater. **11**, 2002326 (2021)

126. B. Zhang, G. Lyu, E.A. Kelly, R.C. Evans, Förster resonance energy transfer in luminescent solar concentrators. Adv. Sci. **9**, 2201160 (2022)

127. K. Kim, S.K. Nam, J. Cho, J.H. Moon, Photon upconversion-assisted dual-band luminescence solar concentrators coupled with perovskite solar cells for highly efficient semi-transparent photovoltaic systems. Nanoscale **12**, 12426 (2020)

128. L. Xu, Y. Yao, N.D. Bronstein, L. Li, A.P. Alivisatos, R.G. Nuzzo, Enhanced photon collection in luminescent solar concentrators with distributed bragg reflectors. ACS Photonics **3**, 278 (2016)

129. J. Gutmann, M. Peters, B. Bläsi, M. Hermle, A. Gombert, H. Zappe, J.C. Goldschmidt, Electromagnetic simulations of a photonic luminescent solar concentrator. Opt. Express **20**, A157 (2012)

130. H.C. Bauser, C.R. Bukowsky, M. Phelan, W. Weigand, D.R. Needell, Z.C. Holman, H.A. Atwater, Photonic crystal waveguides for> 90% light trapping efficiency in luminescent solar concentrators. ACS Photon. **7**, 2122 (2020)

131. K. Park, J. Yi, S.-Y. Yoon, S.M. Park, J. Kim, H.-B. Shin, S. Biswas, G.Y. Yoo, S.-H. Moon, J. Kim, Luminescent solar concentrator efficiency enhanced via nearly lossless propagation pathways. Nat. Photon. (2024). https://doi.org/10.1038/s41566-024-01502-2

132. K. Wu, H. Li, V.I. Klimov, Tandem luminescent solar concentrators based on engineered quantum dots. Nat. Photon. **12**, 105 (2018)

133. D.M. de Clercq, S.V. Chan, J. Hardy, M.B. Price, N.J. Davis, Reducing reabsorption in luminescent solar concentrators with a self-assembling polymer matrix. J. Lumin. **236**, 118095 (2021)

134. C.-S. Huang, K. Jakubowski, S. Ulrich, S. Yakunin, M. Clerc, C. Toncelli, R.M. Rossi, M.V. Kovalenko, L.F. Boesel, Nano-domains assisted energy transfer in amphiphilic polymer conetworks for wearable luminescent solar concentrators. Nano Energy **76**, 105039 (2020)

135. C. Tummeltshammer, M. Portnoi, S.A. Mitchell, A.-T. Lee, A.J. Kenyon, A.B. Tabor, I. Papakonstantinou, On the ability of förster resonance energy transfer to enhance luminescent solar concentrator efficiency. Nano Energy **32**, 263 (2017)

136. S. Saeidi, B. Rezaei, N. Irannejad, A.A. Ensafi, Efficiency improvement of luminescent solar concentrators using upconversion nitrogen-doped graphene quantum dots. J. Power. Sources **476**, 228647 (2020)

137. S.-J. Ha, J.-H. Kang, D.H. Choi, S.K. Nam, E. Reichmanis, J.H. Moon, Upconversion-assisted dual-band luminescent solar concentrator coupled for high power conversion efficiency photovoltaic systems. ACS Photon. **5**, 3621 (2018)

138. J.C. Goldschmidt, M. Peters, A. Bösch, H. Helmers, F. Dimroth, S.W. Glunz, G. Willeke, Increasing the efficiency of fluorescent concentrator systems. Sol. Energy Mater. Sol. Cells **93**, 176 (2009)

139. C.N. Eisler, L.E. Parsons, Z. Nett, C. Love, A.M. Schwartzberg, A.P. Alivisatos, Photonic luminescent solar concentrator design for high efficiency, low cost multijunction photovoltaics. Front. Photon. **3**, 932913 (2022)

140. F. Mateen, M. Ali, H. Oh, S.-K. Hong, Nitrogen-doped carbon quantum dot based luminescent solar concentrator coupled with polymer dispersed liquid crystal device for smart management of solar spectrum. Sol. Energy **178**, 48 (2019)

141. R. Zohrabi, A. Namdar, S. Ahmadi-Kandjani, B. Olyaeefar, Influence of the graded index cholesteric liquid crystal reflectors on the luminescent solar concentrator efficiency. Int. J. Opt. Photon. **16**, 211 (2022)

142. M. Cao, X. Zhao, X. Gong, Achieving high-efficiency large-area luminescent solar concentrators. JACS Au **3**, 25 (2023)

143. Y. Han, X. Zhao, A. Vomiero, X. Gong, H. Zhao, Red and green-emitting biocompatible carbon quantum dots for efficient tandem luminescent solar concentrators. J. Mater. Chem. C **9**, 12255 (2021)

144. G. Liu, H. Zhao, F. Diao, Z. Ling, Y. Wang, Stable tandem luminescent solar concentrators based on cdse/cds quantum dots and carbon dots. J. Mater. Chem. C **6**, 10059 (2018)

145. R. Zarcone, M. Brocato, P. Bernardoni, D. Vincenzi, Building integrated photovoltaic system for a solar infrastructure: Livlib'project. Energy Proced. **91**, 887 (2016)

146. N.S. Makarov, D. Korus, D. Freppon, K. Ramasamy, D.W. Houck, A. Velarde, A. Parameswar, M.R. Bergren, H. McDaniel, Minimizing scaling losses in high-performance quantum dot luminescent solar concentrators for large-area solar windows. ACS Appl. Mater. Interfaces **14**, 29679 (2022)

147. D.E. Smith, M.D. Hughes, D.-A. Borca-Tasciuc, Towards a standard approach for annual energy production of concentrator-based building-integrated photovoltaics. Renew. Energy **186**, 469 (2022)

148. M. Kanellis, M.M. de Jong, L. Slooff, M.G. Debije, The solar noise barrier project: 1 Effect of incident light orientation on the performance of a large-scale luminescent solar concentrator noise barrier. Renew. Energy **103**, 647 (2017)

149. T.A. de Bruin, R. Terricabres-Polo, A. Kaul, N.K. Zawacka, P.T. Prins, T.F. Gietema, A.C. de Waal, D.K. de Boer, D.A. Vanmaekelbergh, P. Leblans, Analysis of the 1 year outdoor performance of quantum dot luminescent solar concentrators. Solar RRL **7**, 2201121 (2023)

150. G. Li, Q. Xuan, M. Akram, Y.G. Akhlaghi, H. Liu, S. Shittu, Building integrated solar concentrating systems: a review. Appl. Energy **260**, 114288 (2020)

151. F. Meinardi, F. Bruni, S. Brovelli, Luminescent solar concentrators for building-integrated photovoltaics. Nat. Rev. Mater. **2**, 1 (2017)

152. A. Reinders, M.G. Debije, A. Rosemann, Measured efficiency of a luminescent solar concentrator pv module called leaf roof. IEEE J. Photovolt. **7**, 1663 (2017)

153. A. Reinders, N. Ekins-Daukes, T. Schmidt, H. Yang, M. Michalska, R. Pelosi, M. Nitti, L. Gillan, D. McCamey, E. M. Gholizadeh, Designing with luminescent solar concentrator photovoltaics, *2019 IEEE 46th Photovoltaic Specialists Conference (PVSC)*, IEEE, pp. 0221–0226 (2019).

154. A. Renny, C. Yang, R. Anthony, R.R. Lunt, Luminescent solar concentrator paintings: Connecting art and energy. J. Chem. Educ. **95**, 1161 (2018)

155. J. Ko, C. Kim, D. Lee, S. Lee, W.G. Shin, G.H. Kang, J. Oh, S.W. Ko, H.-J. Song, Real-time detection and classification of bypass diode-related faults in photovoltaic modules via thermoelectric devices. Adv. Mater. Technol. **9**, 2301209 (2024)

156. L. Fauzan, M.J. Yun, Y.H. Sim, D.Y. Lee, S.I. Cha, Small area high voltage photovoltaic module for high tolerance to partial shading. iScience **26**, 106745 (2023)

157. M. Portnoi, P.A. Haigh, T.J. Macdonald, F. Ambroz, I.P. Parkin, I. Darwazeh, I. Papakonstantinou, Bandwidth limits of luminescent solar concentrators as detectors in free-space optical communication systems. Light Sci. Appl. (2021). https://doi.org/10.1038/s41377-020-00444-y

158. C.H. Parrish, D. Hebert, A. Jackson, K. Ramasamy, H. McDaniel, G.A. Giacomelli, M.R. Bergren, Optimizing spectral quality with quantum dots to enhance crop yield in controlled environments. Commun. Biol. **4**, 124 (2021)

159. G. Liu, B. Sun, H. Li, Y. Wang, H. Zhao, Integration of photoelectrochemical devices and luminescent solar concentrators based on giant quantum dots for highly stable hydrogen generation. J. Mater. Chem. A **7**, 18529 (2019)

160. F. Meinardi, F. Bruni, C. Castellan, M. Meucci, A.M. Umair, M. La Rosa, J. Catani, S. Brovelli, Certification grade quantum dot luminescent solar concentrator glazing with optical wireless communication capability for connected sustainable architecture. Adv. Energy Mater. **14**, 2304006 (2024)

161. Y. Jiang, X. Zhang, G. Wei, Z. Su, Fabrication, material regulation, and healthcare applications of flexible photodetectors. J. Mater. Chem. C **10**, 12511 (2022)

162. M. Raeisossadati, N.R. Moheimani, D. Parlevliet, Red luminescent solar concentrators to enhance scenedesmus sp Biomass productivity. Algal Res. **45**, 101771 (2020)

163. M. Raeisossadati, N.R. Moheimani, Can luminescent solar concentrators increase microalgal growth on anaerobically digested food effluent? J. Appl. Phycol. **32**, 3703 (2020)

164. N. Talebzadeh, P.G. O'Brien, Elliptic array luminescent solar concentrators for combined power generation and microalgae growth. Energies **14**, 5229 (2021)

165. A. Vilanova, P. Dias, T. Lopes, A. Mendes, The route for commercial photoelectrochemical water splitting: a review of large-area devices and key upscaling challenges. Chem. Soc. Rev. (2024). https://doi.org/10.1039/d1cs01069g